석사 학위논문

Master's Thesis

고차 잔류 유연도를 고려한 부분 구조 합성법 개발

Development of a component mode synthesis method with higher-order residual flexibility

김 재 민(金 在 珉 Kim, Jaemin)

기계항공공학부 해양시스템 대학원

School of Mechanical and Aerospace Engineering
Graduate School of Ocean Systems Engineering

KAIST

2016

고차 잔류 유연도를 고려한 부분 구조 합성법 개발

Development of a component mode synthesis method with higher-order residual flexibility

Development of a component mode synthesis method with higher-order residual flexibility

Advisor : Professor Lee, Phill-Seung

by

Kim, Jaemin
School of Mechanical and Aerospace Engineering
Graduate School of Ocean Systems Engineering
KAIST

A thesis submitted to the faculty of KAIST in partial fulfillment of the requirements for the degree of Master of Science in Engineering in the School of Mechanical and Aerospace Engineering, Graduate School of Ocean Systems Engineering. The study was conducted in accordance with Code of Research Ethics[1]

2015, 12, 07
Approved by
Professor Lee, Phill-Seung

[1]Declaration of Ethical Conduct in Research**:** I, as a graduate student of KAIST, hereby declare that I have not committed any acts that may damage the credibility of my research. These include, but are not limited to: falsification, thesis written by someone else, distortion of research findings or plagiarism. I affirm that my thesis contains honest conclusions based on my own careful research under the guidance of my thesis advisor.

Development of a component mode synthesis method with higher-order residual flexibility

Kim, Jaemin

The present dissertation has been approved by the dissertation committee as a master's thesis at KAIST

2015. 12. 07.

Committee head Lee, Phill-Seung _____

Committee member Lee, Byung-Chai _____

Committee member Han, Jae-Hung _____

MOSE
20143161

김 재 민. Kim, Jaemin. Development of a component mode synthesis method with higher-order residual flexibility. 고차 잔류 유연도를 고려한 부분 구조 합성법 개발. School of Mechanical and Aerospace Engineering, Graduate School of Ocean Systems Engineering. 2016. 44 p. Advisor Prof. Lee, Phill-Seung. Text in English.

ABSTRACT

In this paper, we improve the Craig-Bampton (CB) method, one of most widely used component mode synthesis (CMS) methods. Considering the higher-order effect of residual modes that are simply truncated in the CB method, a new transformation matrix is developed. Using the transformation matrix in the CB method (higher-order CB method: HCB), the original finite element model can be more accurately reduced. In the formulation, unknown eigenvalues are considered as additional generalized coordinates, which can be eliminated using SEREP (system equivalent reduction expansion process). We here present the formulation of the higher-order CB method and demonstrate its excellent performance through various examples.

Keywords: Structural dynamics; Finite element method; Model reduction; Component mode synthesis; Craig-Bampton method

Contents

Abstract ····· i

Contents ····· ii

List of Tables ····· iii

List of Figures ····· iv

Chapter 1. Introduction ····· 1

Chapter 2. Dynamic condensation ····· 3

2.1 General description ····· 3

2.2 Guyan reduction ····· 5

2.3 Improved reduced system (IRS) ····· 7

2.4 System Equivalent Reduction Expansion Process (SEREP) ····· 9

Chapter 3. Component mode synthesis ····· 11

3.1 General description ····· 11

3.2 Craig-Bampton (CB) method ····· 14

3.3 Enhanced Craig-Bampton (ECB) method ····· 17

Chapter 4. Higher-order Craig-Bampton method

4.1 Formulations ····· 20

4.2 Numerical examples ····· 24

4.2.1 Rectangular plate problem ····· 24

4.2.2 Cylindrical solid problem ····· 30

4.2.3 Cylindrical panel problem ····· 33

4.2.4 Hyperboloid problem ····· 36

Chapter 5. Computational cost ····· 39

Chapter 6. Conclusion ····· 42

References ····· 43

Summary (in Korean) ····· 45

List of Tables

4.1 The number of dominant modes for the rectangular plate problem 1 ····· 25

4.2 The relative eigenvalue errors for the rectangular plate problem 1 ····· 28

4.3 The relative eigenvector errors for the rectangular plate problem 1 ····· 29

4.4 The number of dominant modes for the cylindrical solid problem ····· 30

4.5 The number of dominant modes for the cylindrical panel problem ····· 33

4.6 The number of dominant modes for the hyperboloid shell problem ····· 36

5.1 The number of dominant modes for the rectangular plate problem 2 ····· 39

5.2 Computation cost for the rectangular plate problem 2 ····· 41

List of Figures

2.1 DOFs selection in a rectangular plate problem ····· 3

3.1 Partitioning procedures in Craig-Bampton method ····· 12

4.1 Rectangular plate problem 1 ····· 26

4.2 Numerical results for the rectangular plate problem 1 ····· 27

4.3 Cylindrical solid problem ····· 31

4.4 Numerical results for the cylindrical solid problem ····· 32

4.5 Cylindrical panel problem with a distorted mesh ····· 34

4.6 Numerical results for the cylindrical panel problem ····· 35

4.7 Hyperboloid shell problem ····· 37

4.8 Numerical results for the hyperboloid shell problem ····· 38

5.1 Rectangular plate problem 2 ····· 40

5.2 Relative eigenvalue errors for the rectangular plate problem 2 ····· 40

Chapter 1. Introduction

In structural dynamics, finite element (FE) method has been widely used to analysis dynamic response. Along with enormous improvement of computer modeling technologies, the FE model has been rapidly larger and complicated. For this reason, it is desirable to develop methods for analyzing and reducing substructures of a FE model. Such methods have been known as dynamic condensation, which is based on DOFs selection, and component mode synthesis (CMS), which is based on modes selection.

In dynamic condensation, the DOFs of global (original) FE model is divided into two parts, “master” DOFs to be retained and “slave” DOFs to be eliminated. The fundamental assumption of dynamic condensa-tion is that the master DOFs dominate the slave DOFs. In other words, it is possible that the global behavior can be approximated by using master DOFs which is only small portion of total DOFs. In 1965, Guyan [1] and Iron [2] first proposed the dynamic condensation method, which is generally called Guyan reduction. Since then, various dynamic condensation methods have been developed such as improved reduced system (IRS) [3], system equivalent reduction expansion process (SEREP) [4]. Recent studies have focused on development of iterative procedure such as iterated-IRS (IIRS) [5].

In component mode synthesis (CMS), the global FE model is partitioned into several substructures by boundary-interface treatments. Using modal analysis, each substructure can be approximated by its dominant substructural modes which is small portion of total modes. By assembling dominant substructural modes and boundary interface, we can obtain reduced FE model. After Hurty’s pioneering works in 1965 [8], a number of CMS methods have been developed. An important milestone is the Craig and Bampton’s work [9], in which a simple and effective CMS method, namely the CB method, was proposed. Then, a various of CMS methods were introduced by Craig and Chang, Benfield, MacNeal, Rubin and Rixen [10-23].

Among various CMS and dynamic condensation methods and developed, the CB method has been widely adopted in many engineering applications. This is because CB method has several advantages that it leads to

easier formulation, high accuracy, high reliability and computational efficiency [15]. In the CB method, each substructure and its component modes are obtained by fixing all its boundary degrees of freedom (DOFs) and it is assumed that each substructural displacement can be approximated by a significantly smaller set of component modes, which is obtained by truncating high modes, or residual modes [6].

Recently, the CB method was significantly improved by Kim and Lee [20]. The new method is named the enhanced CB method (ECB). The key idea is to consider the first-order effect of residual flexibility, which is complement set of residual modes [6,19,20], in the transformation matrix. In the ECB formulation, residual flexibility is represented by Taylor expansion which has unknown eigenvalues. Importantly, the unknown eigenvalues are approximated by adopting O'Callahan's idea [3]. Then, a question arises. What happens if the second-, third-, or higher-order effect of residual modes are considered?

In this study, our focus is on the consideration of the higher-order effect of residual flexibility, leading to improve the accuracy of the CB method. In the ECB method, unknown eigenvalues of first-order residual flexibility are approximated using O'Callahan's idea; however, it is not easy to handle unknown eigenvalues of higher-order residual flexibilities using O'Callahan's idea. Thus, we propose a new method to handle with unknown eigenvalues of higher-order terms. The new method is named the higher-order CB method (HCB). In the HCB method, generalized coordinates are newly defined, which contains unknown eigenvalues, and the higher-order effect of residual flexibility, of which variables are all known, is consider in the transformation matrix. The generalized coordinates which contains unknown eigenvalues are eliminated by SEREP.

In Chapter 2 and Chapter 3, we briefly review the dynamic condensation methods and CMS methods. In Chapter 4, we proposed a new CMS method by improving the CB method (HCB). The performance of HCB method is verified through various numerical examples: rectangular plate, cylindrical solid, cylindrical panel and hyperboloid shell problems.

Chapter 2. Dynamic condensation

2.1 General description

Dynamic equations of motion for free vibration analysis can be represented by

$$\mathbf{M}_g\ddot{\mathbf{u}}_g + \mathbf{K}_g\mathbf{u}_g = \mathbf{0} \tag{2.1}$$

where $\mathbf{M}_g$ and $\mathbf{K}_g$ are mass and stiffness matrices, respectively, and $\mathbf{u}_g$ is the displacement vector. $\mathbf{M}_g$, $\mathbf{K}_g$ and $\mathbf{u}_g$ can be partitioned as

$$\mathbf{M}_g = \begin{bmatrix} \mathbf{M}_a & \mathbf{M}_c \\ \mathbf{M}_c^T & \mathbf{M}_d \end{bmatrix},\ \mathbf{K}_g = \begin{bmatrix} \mathbf{K}_a & \mathbf{K}_c \\ \mathbf{K}_c^T & \mathbf{K}_d \end{bmatrix},\ \mathbf{u}_g = \begin{Bmatrix} \mathbf{u}_a \\ \mathbf{u}_d \end{Bmatrix}, \tag{2.2}$$

where subscript *g*, *a*, *d* and *c* denote global (exact), activated, deleted and coupled quantities corresponding to their DOFs. Then the generalized eigenvalue problem is

$$\mathbf{K}_g\{\boldsymbol{\varphi}_g\}_j = (\lambda_g)_j\mathbf{M}_g\{\boldsymbol{\varphi}_g\}_j,\quad j = 1, 2, \cdots, N_g, \tag{2.3}$$

where $(\lambda_g)_j$ and $\{\boldsymbol{\varphi}_g\}_j$ are the j^{th} global eigenvalue and eigenvector, respectively, and N_g is the number of DOFs in the global structure.

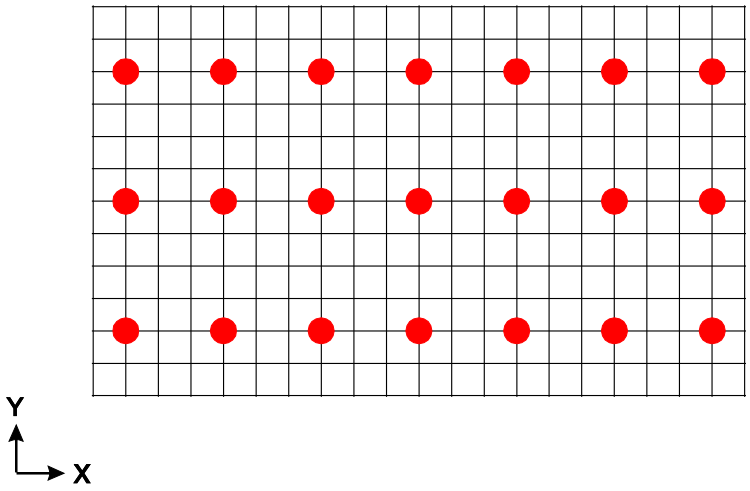

Fig. 2.1. DOFs selection in a rectangular plate problem: red points are activated DOFs and the other points are deleted DOFs

In structural dynamics, the eigenvalues and eigenvectors are interpreted as natural frequency and corresponding mode shape. Note that each eigenvector has a unique mode shape but arbitrary amplitude. Thus, it is convenient to normalize the eigenvectors with respect to mass as follows:

$$\{\boldsymbol{\varphi}_g\}_i^T \mathbf{M}_g \{\boldsymbol{\varphi}_g\}_j = \delta_{ij} \quad \text{for} \quad i \quad \text{and} \quad j = 1, 2, \cdots, N_g, \tag{2.4a}$$

$$\{\boldsymbol{\varphi}_g\}_i^T \mathbf{K}_g \{\boldsymbol{\varphi}_g\}_j = (\lambda_g)_j \delta_{ij} \quad \text{for} \quad i \quad \text{and} \quad j = 1, 2, \cdots, N_g, \tag{2.4b}$$

where δ_{ij} is Kronecker delta ($\delta_{ij} = 1$ if $i = j$, otherwise $\delta_{ij} = 0$). Eq. (2.4a) and Eq. (2.4b) are also called mass-orthonormality and stiffness-orthogonality, respectively.

Using the eigenvectors, the global displacement $\mathbf{u}_g$ is represented by

$$\mathbf{u}_g = \boldsymbol{\Phi}_g \mathbf{q}_g, \tag{2.5a}$$

$$\boldsymbol{\Phi}_g = [\{\boldsymbol{\varphi}_g\}_1 \quad \{\boldsymbol{\varphi}_g\}_2 \quad \cdots \quad \{\boldsymbol{\varphi}_g\}_{N_g}], \tag{2.5b}$$

where $\boldsymbol{\Phi}_g$ and $\mathbf{q}_g$ are the global transformation matrix and its generalized coordinate vector, respectively.

In dynamic condensation, global DOFs are divide into two parts, activated DOFs to be retained and deleted DOFs to be eliminated. Thus, the generalized eigenvalue problem can be reduced as

$$\mathbf{K}_a \{\overline{\boldsymbol{\varphi}}_a\}_j = (\overline{\lambda}_a)_j \mathbf{M}_a \{\overline{\boldsymbol{\varphi}}_a\}_j \quad \text{for} \quad j = 1, 2, \cdots, N_a, \tag{2.6}$$

where $(\overline{\lambda}_a)_j$ and $\{\overline{\boldsymbol{\varphi}}_a\}_j$ are the j^{th} approximated eigenvalue and eigenvector, respectively, and N_a is the number of DOFs in the reduced structure. Here, *m* denotes master quantities corresponding to master DOFs and an overbar $\overline{(\ )}$ denotes approximated quantities.

Finally, using the approximated eigenvectors, the global displacement $\mathbf{u}_g$ is approximated by

$$\mathbf{u}_g \approx \overline{\mathbf{u}}_a = \overline{\boldsymbol{\Phi}}_a \overline{\mathbf{q}}_a, \tag{2.7a}$$

$$\overline{\boldsymbol{\Phi}}_a = [\{\overline{\boldsymbol{\varphi}}_a\}_1 \quad \{\overline{\boldsymbol{\varphi}}_a\}_2 \quad \cdots \quad \{\overline{\boldsymbol{\varphi}}_a\}_{N_a}], \tag{2.7b}$$

where $\overline{\boldsymbol{\Phi}}_a$ and $\overline{\mathbf{q}}_a$ are the reduced transformation matrix and its generalized coordinate vector, respectively.

2.2 Guyan reduction

In Guyan reduction, the transformation matrix for dynamic condensation was developed based on the static analysis [1]. By neglecting the mass matrix in Eq. (2.1), the static equations of motion can be obtained by

$$\mathbf{K}_g \mathbf{u}_g = \mathbf{0}, \tag{2.8a}$$

$$\mathbf{K}_g = \begin{bmatrix} \mathbf{K}_a & \mathbf{K}_c \\ \mathbf{K}_c^T & \mathbf{K}_d \end{bmatrix}, \ \mathbf{u}_g = \begin{Bmatrix} \mathbf{u}_a \\ \mathbf{u}_d \end{Bmatrix}. \tag{2.8b}$$

From the second row in Eq. (2.8), we can obtain following relation

$$\mathbf{K}_c^T \mathbf{u}_a + \mathbf{K}_d \mathbf{u}_d = \mathbf{0}, \tag{2.9a}$$

$$\mathbf{u}_a = -\mathbf{K}_d^{-1} \mathbf{K}_c^T \mathbf{u}_a. \tag{2.9b}$$

By substituting Eq. (2.9b) into Eq. (2.8a) and neglecting the deleted DOFs,

$$\mathbf{u}_g \approx \overline{\mathbf{u}}_g = \overline{\mathbf{T}}_G \mathbf{u}_a, \tag{2.10a}$$

$$\overline{\mathbf{T}}_G = \begin{bmatrix} \mathbf{I} \\ -\mathbf{K}_d^{-1} \mathbf{K}_c^T \end{bmatrix}, \tag{2.10b}$$

where $\overline{\mathbf{T}}_G$ is the transformation matrix of Guyan reduction. Here, subscript *G* denotes the quantities corresponding to Guyan transformation.

Using the transformation matrix $\overline{\mathbf{T}}_G$, the reduced model obtained by

$$\overline{\mathbf{M}}_G = \overline{\mathbf{T}}_G^T \mathbf{M}_g \overline{\mathbf{T}}_G, \ \overline{\mathbf{K}}_G = \overline{\mathbf{T}}_G^T \mathbf{K}_g \overline{\mathbf{T}}_G, \tag{2.11}$$

where $\overline{\mathbf{M}}_G$ and $\overline{\mathbf{K}}_G$ are the reduced component mass and stiffness matrices, respectively.

Using the results of Eq. (2.11), the reduced eigenvalue problem can be obtained by

$$\overline{\mathbf{K}}_G \{\overline{\boldsymbol{\varphi}}_G\}_j = (\overline{\lambda}_G)_j \overline{\mathbf{M}}_G \{\overline{\boldsymbol{\varphi}}_G\}_j \ \text{ for } \ j = 1, 2, \cdots, N_a, \tag{2.12}$$

where $(\overline{\lambda}_G)_j$ and $\{\overline{\boldsymbol{\varphi}}_G\}_j$ are the j^{th} approximated eigenvalue and eigenvector, respectively, and N_a is the number of activated DOFs, which is the size of the reduced system.

Finally, using the approximated eigenvectors, the global displacement $\mathbf{u}_g$ is approximated by

$$\mathbf{u}_g \approx \overline{\mathbf{u}}_G = \overline{\mathbf{\Phi}}_G \overline{\mathbf{q}}_G, \tag{2.13a}$$

$$\overline{\mathbf{\Phi}}_G = [\{\overline{\boldsymbol{\varphi}}_G\}_1 \quad \{\overline{\boldsymbol{\varphi}}_G\}_2 \quad \cdots \quad \{\overline{\boldsymbol{\varphi}}_G\}_{N_a}], \tag{2.13b}$$

where $\overline{\mathbf{\Phi}}_G$ and $\overline{\mathbf{q}}_G$ are the reduced transformation matrix and its generalized coordinate vector in Guyan reduction, respectively.

2.3 Improved reduced system (IRS)

In IRS reduction, the transformation matrix for dynamic condensation was developed based on the dynamic analysis [3]. From Eq. (2.2) and Eq. (2.3), the partitioned eigenvalue problem of global structure can be written by

$$\begin{bmatrix} \mathbf{K}_a & \mathbf{K}_c \\ \mathbf{K}_c^T & \mathbf{K}_d \end{bmatrix} \begin{Bmatrix} \mathbf{u}_a \\ \mathbf{u}_d \end{Bmatrix} = \lambda_g \begin{bmatrix} \mathbf{M}_a & \mathbf{M}_c \\ \mathbf{M}_c^T & \mathbf{M}_d \end{bmatrix} \begin{Bmatrix} \mathbf{u}_a \\ \mathbf{u}_d \end{Bmatrix}. \tag{2.14}$$

From the second row in Eq. (2.14), the following relation can be obtained by

$$\mathbf{K}_c^T \mathbf{u}_a + \mathbf{K}_d \mathbf{u}_d = \lambda_g [\mathbf{M}_c^T \mathbf{u}_a + \mathbf{M}_d \mathbf{u}_d], \tag{2.15a}$$

$$\mathbf{u}_d = [\mathbf{K}_d - \lambda_g \mathbf{M}_d]^{-1} [\lambda_g \mathbf{M}_c^T - \mathbf{K}_c^T] \mathbf{u}_a. \tag{2.15b}$$

By substituting Eq. (2.15b) into Eq. (2.14a) and neglecting the deleted DOFs,

$$[\mathbf{K}_a - \lambda_g \mathbf{M}_a - [\mathbf{K}_c - \lambda_g \mathbf{M}_c][\mathbf{K}_d - \lambda_g \mathbf{M}_d]^{-1} [\mathbf{K}_c^T - \lambda_g \mathbf{M}_c^T]] \mathbf{u}_a = \mathbf{0}. \tag{2.16}$$

Note that Eq. (2.16) is the reduced eigenvalue problem which has exact solution. However, it is difficult to solve the Eq. (2.16) because of unknown eigenvalue λ_g.

To handle λ_g easily, inverse term in Eq. (2.16) can be expanded as

$$[\mathbf{K}_d - \lambda_g \mathbf{M}_d]^{-1} = \mathbf{K}_d^{-1} + \lambda_g \mathbf{K}_d^{-1} \mathbf{M}_d \mathbf{K}_d^{-1} + O(\lambda_g^2) + O(\lambda_g^3) + \cdots. \tag{2.17}$$

By substituting Eq. (2.17) into Eq. (2.15b) and neglecting higher order terms of λ_g, $\mathbf{u}_a$ can be approximated by

$$\mathbf{u}_a \approx -\mathbf{K}_a^{-1} \mathbf{K}_c^T \mathbf{u}_a + \lambda_g [\mathbf{K}_a^{-1} \mathbf{M}_c^T - \mathbf{K}_a^{-1} \mathbf{M}_a \mathbf{K}_a^{-1} \mathbf{K}_c^T] \mathbf{u}_a. \tag{2.18}$$

O'callahan [3] proposed that λ_g can be approximated by the component matrices of Guyan reduction.

$$\lambda_g \mathbf{u}_a \approx \overline{\lambda}_G \mathbf{u}_a = \overline{\mathbf{M}}_G^{-1} \overline{\mathbf{K}}_G \mathbf{u}_a. \tag{2.19}$$

By substituting Eq. (2.19) into Eq. (2.18), the global displacement $\mathbf{u}_g$ can be approximated by

$$\mathbf{u}_g \approx \overline{\mathbf{u}}_g = \overline{\mathbf{T}}_{IRS}\mathbf{u}_a , \tag{2.20a}$$

$$\overline{\mathbf{T}}_{IRS} = \begin{bmatrix} \mathbf{I} \\ -\mathbf{K}_a^{-1}\mathbf{K}_c^T + [\mathbf{K}_a^{-1}\mathbf{M}_c^T - \mathbf{K}_a^{-1}\mathbf{M}_a\mathbf{K}_a^{-1}\mathbf{K}_c^T]\overline{\mathbf{M}}_G^{-1}\overline{\mathbf{K}}_G \end{bmatrix}. \tag{2.20b}$$

Using the transformation matrix $\overline{\mathbf{T}}_{IRS}$, the reduced model obtained by

$$\overline{\mathbf{K}}_{IRS} = \overline{\mathbf{T}}_{IRS}^T\mathbf{K}_g\overline{\mathbf{T}}_{IRS}, \quad \overline{\mathbf{M}}_{IRS} = \overline{\mathbf{T}}_{IRS}^T\mathbf{M}_g\overline{\mathbf{T}}_{IRS}, \tag{2.21}$$

where $\overline{\mathbf{M}}_{IRS}$ and $\overline{\mathbf{K}}_{IRS}$ are the reduced component mass and stiffness matrices, respectively.

Reduced eigenvalue problem can be obtained by

$$\overline{\mathbf{K}}_{IRS}\{\overline{\boldsymbol{\varphi}}_{IRS}\}_j = (\overline{\lambda}_{IRS})_j\overline{\mathbf{M}}_{IRS}\{\overline{\boldsymbol{\varphi}}_{IRS}\}_j \quad \text{for} \quad j = 1, 2, \cdots, N_a , \tag{2.22}$$

where $(\overline{\lambda}_{IRS})_j$ and $\{\overline{\boldsymbol{\varphi}}_{IRS}\}_j$ are the j^{th} approximated eigenvalue and eigenvector, respectively, and N_a is the number of DOFs in the reduced structure.

Finally, using the approximated eigenvectors, the global displacement $\mathbf{u}_g$ is approximated by

$$\mathbf{u}_g \approx \overline{\mathbf{u}}_{IRS} = \overline{\boldsymbol{\Phi}}_{IRS}\overline{\mathbf{q}}_{IRS} , \tag{2.23a}$$

$$\overline{\boldsymbol{\Phi}}_{IRS} = [\{\overline{\boldsymbol{\varphi}}_{IRS}\}_1 \quad \{\overline{\boldsymbol{\varphi}}_{IRS}\}_2 \quad \cdots \quad \{\overline{\boldsymbol{\varphi}}_{IRS}\}_{N_a}] , \tag{2.23b}$$

where $\overline{\boldsymbol{\Phi}}_{IRS}$ and $\overline{\mathbf{q}}_{IRS}$ are the reduced transformation matrix and its generalized coordinate vector in IRS reduction, respectively.

2.4 System equivalent reduction expansion process (SEREP)

From the Eq. (2.5a) and Eq. (2.5b), the global displacement $\mathbf{u}_g$ can be approximated by

$$\mathbf{u}_g = \overline{\mathbf{\Phi}}_g \overline{\mathbf{q}}_g, \tag{2.24a}$$

$$\overline{\mathbf{\Phi}}_g = [\{\boldsymbol{\varphi}_g\}_1 \quad \cdots \quad \{\boldsymbol{\varphi}_g\}_{N_m}], \tag{2.24b}$$

where $\overline{\mathbf{\Phi}}_g$ and $\overline{\mathbf{q}}_g$ are the approximated transformation matrix and its generalized coordinate vector, respectively, and N_m denote the number of modal vectors. Note that columns of $\overline{\mathbf{\Phi}}_g$ are linearly independent and therefore, rank of $\overline{\mathbf{\Phi}}_g$ is N_m.

In SEREP reduction [4], $\mathbf{u}_g$ and $\overline{\mathbf{\Phi}}_g$ are partitioned into two parts, activated and deleted.

$$\mathbf{u}_g = \begin{Bmatrix} \mathbf{u}_a \\ \mathbf{u}_d \end{Bmatrix}, \quad \overline{\mathbf{\Phi}}_g = \begin{bmatrix} \overline{\mathbf{\Phi}}_a \\ \overline{\mathbf{\Phi}}_d \end{bmatrix}, \tag{2.25}$$

where $\mathbf{u}_a$ and $\overline{\mathbf{\Phi}}_a$ are the activated displacement and transformation matrix, respectively, and $\mathbf{u}_d$ and $\overline{\mathbf{\Phi}}_d$ are the deleted displacement and transformation matrix, respectively.

From Eq. (2.24a) and Eq. (2.25), the activated displacement $\mathbf{u}_a$ can be obtained by

$$\mathbf{u}_a = \overline{\mathbf{\Phi}}_a \overline{\mathbf{q}}_g. \tag{2.26}$$

Note that generally N_a is not same with N_m and therefore $\overline{\mathbf{\Phi}}_a$ usually is not a square matrix. For this reason, to solve Eq. (2.26), generalized inverse of $\overline{\mathbf{\Phi}}_a$ is required. There are two case of generalized inverse corresponding to its size.

$$\overline{\mathbf{\Phi}}_a^{ginv} = [\overline{\mathbf{\Phi}}_a^T \overline{\mathbf{\Phi}}_a]^{-1} \overline{\mathbf{\Phi}}_a^T \quad \text{if} \quad N_a \geq N_m, \tag{2.27a}$$

$$\overline{\mathbf{\Phi}}_a^{ginv} = \overline{\mathbf{\Phi}}_a^T [\overline{\mathbf{\Phi}}_a \overline{\mathbf{\Phi}}_a^T]^{-1} \quad \text{if} \quad N_a < N_m. \tag{2.27b}$$

In most practical application, N_a is larger than N_m and therefore, hereafter, we will only handle with the case of Eq. (2.27a).

Using Eq. (2.27a) in Eq. (2.26), following relation is obtained

$$\overline{\mathbf{q}}_g = \overline{\mathbf{\Phi}}_a^{ginv} \mathbf{u}_a. \tag{2.28}$$

By substituting Eq. (2.28) into Eq. (2.24a), following relation is obtained

$$\mathbf{u}_g = \overline{\mathbf{T}}_{SEREP}\mathbf{u}_a, \tag{2.29a}$$

$$\overline{\mathbf{T}}_{SEREP} \equiv \overline{\mathbf{\Phi}}_g \overline{\mathbf{\Phi}}_a^{ginv} = \begin{bmatrix} \overline{\mathbf{\Phi}}_a \overline{\mathbf{\Phi}}_a^{ginv} \\ \overline{\mathbf{\Phi}}_d \overline{\mathbf{\Phi}}_a^{ginv} \end{bmatrix}, \tag{2.29b}$$

where $\overline{\mathbf{T}}_{SEREP}$ is the transformation matrix of SEREP.

Using the transformation matrix $\overline{\mathbf{T}}_{SEREP}$, the reduced model obtained by

$$\overline{\mathbf{K}}_{SEREP} = \overline{\mathbf{T}}_{SEREP}^T \mathbf{K}_g \overline{\mathbf{T}}_{SEREP}, \quad \overline{\mathbf{M}}_{SEREP} = \overline{\mathbf{T}}_{SEREP}^T \mathbf{M}_g \overline{\mathbf{T}}_{SEREP}, \tag{2.30}$$

where $\overline{\mathbf{M}}_{SEREP}$ and $\overline{\mathbf{K}}_{SEREP}$ are the reduced component mass and stiffness matrices, respectively.

Using the results in Eq. (2.30), reduced eigenvalue problem can be obtained by

$$\overline{\mathbf{K}}_{SEREP}\{\overline{\boldsymbol{\varphi}}_{SEREP}\}_j = (\overline{\lambda}_{SEREP})_j \overline{\mathbf{M}}_{SEREP}\{\overline{\boldsymbol{\varphi}}_{SEREP}\}_j \quad \text{for} \quad j = 1, 2, \cdots, N_a, \tag{2.31}$$

where $(\overline{\lambda}_{SEREP})_j$ and $\{\overline{\boldsymbol{\varphi}}_{SEREP}\}_j$ are the j^{th} approximated eigenvalue and eigenvector, respectively, and N_a is the number of DOFs in the reduced structure.

Finally, using the approximated eigenvectors, the global displacement $\mathbf{u}_g$ is approximated by

$$\mathbf{u}_g \approx \overline{\mathbf{u}}_{SEREP} = \overline{\mathbf{\Phi}}_{SEREP}\overline{\mathbf{q}}_{SEREP}, \tag{2.32a}$$

$$\overline{\mathbf{\Phi}}_{SEREP} = [\{\overline{\boldsymbol{\varphi}}_{SEREP}\}_1 \quad \{\overline{\boldsymbol{\varphi}}_{SEREP}\}_2 \quad \cdots \quad \{\overline{\boldsymbol{\varphi}}_{SEREP}\}_{N_a}], \tag{2.32b}$$

where $\overline{\mathbf{\Phi}}_{SEREP}$ and $\overline{\mathbf{q}}_{SEREP}$ are the reduced transformation matrix and its generalized coordinate vector in IRS reduction, respectively.

Note that unlike other reduction methods, transformation of SEREP has no accuracy loss. In other words, eigenvalues of N_a system in Eq. (2.22a) are exactly same with eigenvalues, which are corresponding to activated DOFs, of N_m system in Eq. (2.14a). Thus, following relation are obtained as

$$\mathbf{u}_a = \overline{\mathbf{\Phi}}_{SEREP}\overline{\mathbf{q}}_g, \tag{2.33a}$$

$$\overline{\mathbf{\Phi}}_a = \overline{\mathbf{\Phi}}_{SEREP}. \tag{2.33b}$$

Chapter 3. Component mode synthesis

3.1 General description

Dynamic equations of motion for free vibration analysis can be represented by

$$\mathbf{M}_g\ddot{\mathbf{u}}_g + \mathbf{K}_g\mathbf{u}_g = \mathbf{0}, \tag{3.1}$$

where $\mathbf{M}_g$ and $\mathbf{K}_g$ are mass and stiffness matrices, respectively, $\mathbf{u}_g$ is the displacement vector. Here, subscript *g* denotes global (exact) quantities.

In CMS methods, global structure is partitioned into several substructures and the partitioned $\mathbf{M}_g$, $\mathbf{K}_g$ and $\mathbf{u}_g$ can be represented as

$$\mathbf{M}_g = \begin{bmatrix} \mathbf{M}_s & \mathbf{M}_c \\ \mathbf{M}_c^T & \mathbf{M}_b \end{bmatrix}, \mathbf{M}_s = \begin{bmatrix} \mathbf{M}_s^{(1)} & & \mathbf{0} \\ & \ddots & \\ \mathbf{0} & & \mathbf{M}_s^{(k)} \end{bmatrix}, \ \mathbf{M}_c = \begin{bmatrix} \mathbf{M}_c^{(1)} \\ \vdots \\ \mathbf{M}_c^{(k)} \end{bmatrix}, \tag{3.2a}$$

$$\mathbf{K}_g = \begin{bmatrix} \mathbf{K}_s & \mathbf{K}_c \\ \mathbf{K}_c^T & \mathbf{K}_b \end{bmatrix}, \ \mathbf{K}_s = \begin{bmatrix} \mathbf{K}_s^{(1)} & & \mathbf{0} \\ & \ddots & \\ \mathbf{0} & & \mathbf{K}_s^{(k)} \end{bmatrix}, \ \mathbf{K}_c = \begin{bmatrix} \mathbf{K}_c^{(1)} \\ \vdots \\ \mathbf{K}_c^{(k)} \end{bmatrix}, \tag{3.2b}$$

$$\mathbf{u}_g = \begin{Bmatrix} \mathbf{u}_s \\ \mathbf{u}_b \end{Bmatrix}, \ \mathbf{u}_s = \begin{Bmatrix} \mathbf{u}_s^{(1)} \\ \vdots \\ \mathbf{u}_s^{(k)} \end{Bmatrix} \text{ for } k = 1, 2, \cdots, N_s, \tag{3.2c}$$

where $\mathbf{M}_s^{(k)}$ and $\mathbf{K}_s^{(k)}$ are mass and stiffness matrices of k^{th} substructure, respectively, $\mathbf{u}_s^{(k)}$ is the displacement vector of k^{th} substructure, and N_s is the number of substructures. Here, subscript *s*, *b* and *c* denote structural, boundary and coupled quantities, respectively.

The generalized eigenvalue problems of each substructure are defined by

$$\mathbf{K}_s^{(k)}\{\boldsymbol{\varphi}_s\}_j^{(k)} = (\lambda_s)_j^{(k)}\mathbf{M}_s^{(k)}\{\boldsymbol{\varphi}_s\}_j^{(k)} \text{ for } j = 1, 2, \cdots, N_d^{(k)} \text{ and } k = 1, 2, \cdots, N_s, \tag{3.3}$$

where $(\lambda_s)_j^{(k)}$ and $\{\boldsymbol{\varphi}_s\}_j^{(k)}$ are the j^{th} eigenvalue and eigenvector in k^{th} substructure, respectively, and $N_d^{(k)}$ is the number of dominant eigenvalues in k^{th} substructure.

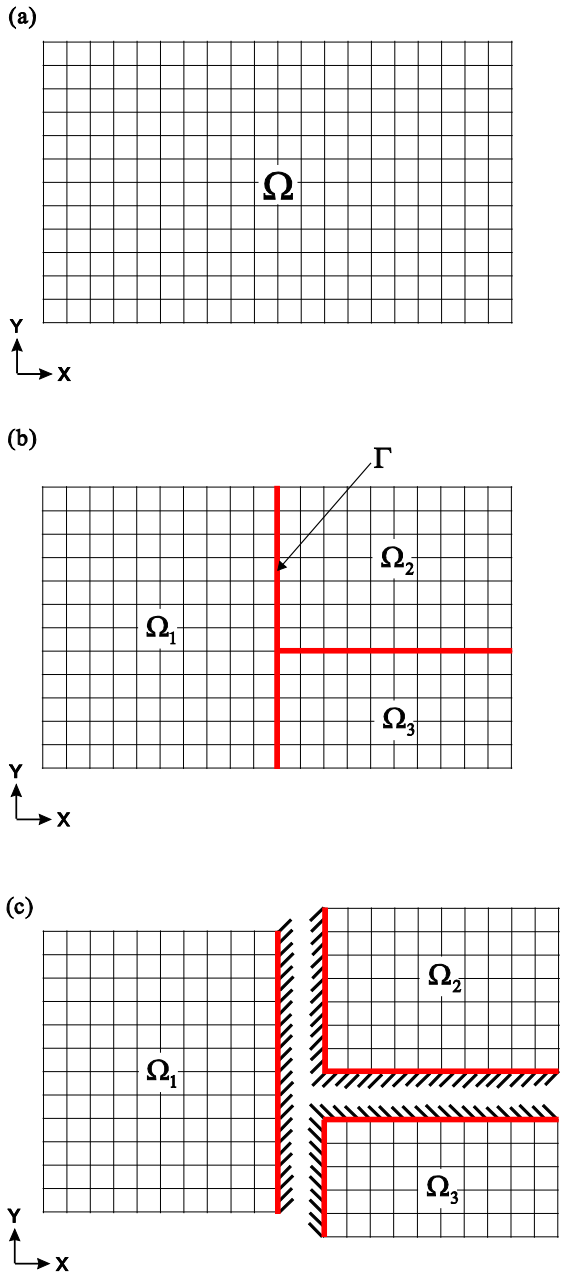

Fig. 3.1. Partitioning procedures in Craig-Bampton method: (a) global FE model (b) partitioned FE models (c) fixed-interface boundary treatment

In structural dynamics, the substructural eigenvalues and eigenvectors are interpreted as substructural natural frequency and corresponding mode shape. Note that each eigenvector has a unique mode shape but arbitrary amplitude. Thus, it is convenient to normalize the eigenvectors with respect to mass as follows:

$$\{\boldsymbol{\varphi}_s^{(k)}\}_i^T \mathbf{M}_s^{(k)} \{\boldsymbol{\varphi}_s^{(k)}\}_j = \delta_{ij} \quad \text{for} \quad i \quad \text{and} \quad j = 1, 2, \cdots, N_d^{(k)}, \quad k = 1, 2, \cdots, N_s, \tag{3.4a}$$

$$\{\boldsymbol{\varphi}_s^{(k)}\}_i^T \mathbf{K}_s^{(k)} \{\boldsymbol{\varphi}_s^{(k)}\}_j = (\lambda_s^{(k)})_j \delta_{ij} \quad \text{for } i \text{ and } j = 1, 2, \cdots, N_d^{(k)}, \ k = 1, 2, \cdots, N_s, \tag{3.4b}$$

where δ_{ij} is Kronecker delta ($\delta_{ij} = 1$ if $i = j$, otherwise $\delta_{ij} = 0$). Eq. (3.6a) and Eq. (3.6b) are also called mass-orthonormality and stiffness-orthogonality, respectively.

In CMS methods, using the substructural eigenvalues and eigenvectors, global displacement vector $\mathbf{u}_g$ can be approximated by

$$\mathbf{u}_g \approx \overline{\mathbf{u}}_g = \overline{\boldsymbol{\Phi}}_g \overline{\mathbf{q}}_g \tag{3.5}$$

where $\overline{\boldsymbol{\Phi}}_g$ and $\overline{\mathbf{q}}_g$ are the reduced transformation matrix and its generalized coordinated vectors, respectively.

Finally, using $\overline{\boldsymbol{\Phi}}_g$, reduced equations of motion is obtained by

$$\overline{\mathbf{M}}_g \ddot{\overline{\mathbf{q}}}_g + \overline{\mathbf{K}}_g \overline{\mathbf{q}}_g = \mathbf{0}, \tag{3.6a}$$

$$\overline{\mathbf{M}}_g = \overline{\boldsymbol{\Phi}}_g^T \mathbf{M}_g \overline{\boldsymbol{\Phi}}_g, \ \overline{\mathbf{K}}_g = \overline{\boldsymbol{\Phi}}_g^T \mathbf{K}_g \overline{\boldsymbol{\Phi}}_g, \tag{3.6b}$$

where $\overline{\mathbf{M}}_g$ and $\overline{\mathbf{K}}_g$ are the reduced mass and stiffness matrices, respectively.

3.2 Craig-Bampton (CB) method

From Eq. (3.1), the global eigenvalue problem is defined

$$\mathbf{K}_g\{\boldsymbol{\varphi}_g\}_j = \lambda_j \mathbf{M}_g\{\boldsymbol{\varphi}_g\}_j \quad \text{for } j = 1, 2, \cdots, N_g, \tag{3.7}$$

where λ_j and $\{\boldsymbol{\varphi}_g\}_j$ are the global eigenvalue and eigenvector, respectively, and N_g is the number of DOFs in the global FE model. In structural dynamics, the eigenvalue and eigenvector can be interpreted as a natural frequency and corresponding mode shape, respectively.

Using the eigenvectors in Eq. (3.8), the global displacement vector $\mathbf{u}_g$ is represented as

$$\mathbf{u}_g = \boldsymbol{\Phi}_g \mathbf{q}_g, \tag{3.8a}$$

$$\boldsymbol{\Phi}_g = [\{\boldsymbol{\varphi}_g\}_1 \quad \{\boldsymbol{\varphi}_g\}_2 \quad \cdots \quad \{\boldsymbol{\varphi}_g\}_{N_g}], \tag{3.8b}$$

$$\mathbf{q}_g = \begin{Bmatrix} \mathbf{q}_1 \\ \mathbf{q}_2 \\ \vdots \\ \mathbf{q}_{N_g} \end{Bmatrix}. \tag{3.8c}$$

In the CB method [9], the global displacement vector $\mathbf{u}_g$ is represented as

$$\mathbf{u}_g = \mathbf{T}_{CB}\mathbf{u}_{CB}, \tag{3.9a}$$

$$\mathbf{T}_{CB} = \begin{bmatrix} \boldsymbol{\Phi}_s & \boldsymbol{\Psi}_c \\ \mathbf{0} & \mathbf{I}_b \end{bmatrix}, \ \mathbf{u}_{CB} = \begin{Bmatrix} \mathbf{q}_s \\ \mathbf{u}_b \end{Bmatrix}, \tag{3.9b}$$

where $\mathbf{T}_{CB}$ and $\mathbf{u}_{CB}$ are the global transformation matrix and its generalized coordinate, $\mathbf{q}_s$ and $\mathbf{u}_b$ are the structural generalized coordinate vector and the boundary displacement vector, respectively, and $\boldsymbol{\Phi}_s$ and $\boldsymbol{\Psi}_c$ are the structural eigenvector matrix and the constraint modes matrix, respectively. Here, the subscript $(\quad)_{CB}$ denotes the partitioned quantities corresponding to CB method.

The structural eigenvector matrix $\boldsymbol{\Phi}_s$ is composed of the substructural eigenvector matrices $\boldsymbol{\Phi}_s^{(k)}$ in block diagonal matrix form. The substructural eigenvector matrices $\boldsymbol{\Phi}_s^{(k)}$ can be determined by substructural eigenvalue problems as follows:

$$\boldsymbol{\Phi}_s = \begin{bmatrix} \boldsymbol{\Phi}_s^{(1)} & & \mathbf{0} \\ & \ddots & \\ \mathbf{0} & & \boldsymbol{\Phi}_s^{(k)} \end{bmatrix} \quad \text{for} \quad k = 1, 2, \cdots, N_s, \tag{3.10a}$$

$$[\mathbf{K}_s^{(k)} - (\lambda_s)_j^{(k)} \mathbf{M}_s^{(k)}]\{\boldsymbol{\varphi}_s\}_j^{(k)} = \mathbf{0} \quad \text{for} \quad j = 1, 2, \cdots, N_s^{(k)}, \tag{3.10b}$$

where N_s is the number of substructures and $N_s^{(k)}$ is the number of deformable modes in the k^{th} substructure, and $(\lambda_s)_j^{(k)}$ and $\{\boldsymbol{\varphi}_s\}_j^{(k)}$ are the j^{th} eigenvalue and eigenvector in k^{th} substructure, respectively.

The constraint mode matrix $\boldsymbol{\Psi}_c$ is composed of the substructural constraint mode matrices $\boldsymbol{\Psi}_c^{(k)}$ in block column matrix form. The substructural constraint mode matrices $\boldsymbol{\Psi}_c^{(k)}$ can be determined by substructural inverse procedure,

$$\boldsymbol{\Psi}_c = \begin{bmatrix} \boldsymbol{\Psi}_c^{(1)} \\ \vdots \\ \boldsymbol{\Psi}_c^{(k)} \end{bmatrix} \quad \text{for} \quad k = 1, 2, \cdots, N_s, \tag{3.11a}$$

$$\boldsymbol{\Psi}_c^{(k)} = -(\mathbf{K}_s^{(k)})^{-1} \mathbf{K}_c, \tag{3.11b}$$

where $\mathbf{K}_s^{(k)}$ is a stiffness matrix of k^{th} substructure and $\mathbf{K}_c$ is a coupled stiffness matrix of global structure.

A fundamental assumption of the CB method is that the mode shape of the global FE model can be approximated by a significantly smaller set of mode shapes corresponding to low frequency. The structural eigenvector matrix $\boldsymbol{\Phi}_s$ can be decomposed into the dominant eigenvector matrix $\boldsymbol{\Phi}_d$ to be retained and the residual eigenvector matrix $\boldsymbol{\Phi}_r$ to be neglected,

$$\mathbf{u}_s = \boldsymbol{\Phi}_s \mathbf{q}_s + \boldsymbol{\Psi}_c \mathbf{u}_b = \begin{bmatrix} \boldsymbol{\Phi}_d & \boldsymbol{\Phi}_r \end{bmatrix} \begin{Bmatrix} \mathbf{q}_d \\ \mathbf{q}_r \end{Bmatrix} + \boldsymbol{\Psi}_c \mathbf{u}_b, \tag{3.12}$$

where $\mathbf{q}_d$ and $\mathbf{q}_r$ are generalized coordinate vectors corresponding to $\boldsymbol{\Phi}_d$ and $\boldsymbol{\Phi}_r$, respectively. Here, the subscripts *d* and *r* denote the dominant and residual quantities.

As neglecting the residual eigenvector matrix $\boldsymbol{\Phi}_r$ in the Eq. (3.12), the global displacement vector $\mathbf{u}_g$ can be approximated by

$$\mathbf{u}_g \approx \overline{\mathbf{u}}_g = \overline{\mathbf{T}}_{CB}\overline{\mathbf{u}}_{CB}, \tag{3.13a}$$

$$\overline{\mathbf{T}}_{CB} = \begin{bmatrix} \boldsymbol{\Phi}_d & \boldsymbol{\Psi}_c \\ \mathbf{0} & \mathbf{I}_b \end{bmatrix}, \ \overline{\mathbf{u}}_{CB} = \begin{Bmatrix} \mathbf{q}_d \\ \mathbf{u}_b \end{Bmatrix}, \tag{3.13b}$$

where $\overline{\mathbf{T}}_{CB}$ and $\overline{\mathbf{u}}_{CB}$ are the reduced transformation matrix and the its generalized coordinate vector, respectively, and $\overline{\mathbf{u}}_g$ is the approximated global displacement. Here, overbar $(\bar{\ })$ denotes the approximated quantities. Note that the residual eigenvector matrix was simply truncated without any consideration in the Eq. (3.13a) and Eq. (3.13b).

Using $\overline{\mathbf{T}}_{CB}$ in Eq. (3.13), we can obtain the reduced equations of motion for partitioned structure,

$$\overline{\mathbf{M}}_{CB}\ddot{\overline{\mathbf{u}}}_{CB} + \overline{\mathbf{K}}_{CB}\overline{\mathbf{u}}_{CB} = \mathbf{0}, \tag{3.14a}$$

$$\overline{\mathbf{M}}_{CB} = \overline{\mathbf{T}}_{CB}^T\mathbf{M}_g\overline{\mathbf{T}}_{CB}, \ \overline{\mathbf{K}}_{CB} = \overline{\mathbf{T}}_{CB}^T\mathbf{K}_g\overline{\mathbf{T}}_{CB}, \tag{3.14b}$$

where $\overline{\mathbf{M}}_{CB}$ and $\overline{\mathbf{K}}_{CB}$ are the reduced mass and stiffness matrices, respectively, and $\overline{\mathbf{u}}_{CB}$ is the reduced displacement vector.

Using $\overline{\mathbf{M}}_{CB}$ and $\overline{\mathbf{K}}_{CB}$ in Eq. (3.14b), the reduced eigenvalue problem can be represented as

$$[\overline{\mathbf{K}}_{CB} - (\overline{\lambda}_{CB})_j\overline{\mathbf{M}}_{CB}]\{\overline{\boldsymbol{\varphi}}_{CB}\}_j = \mathbf{0} \ \text{ for } \ j = 1, 2, \cdots, \overline{N}_{CB}, \tag{3.15}$$

where $(\overline{\lambda}_{CB})_j$ and $\{\overline{\boldsymbol{\varphi}}_{CB}\}_j$ is the j^{th} approximated eigenvalue and eigenvector, respectively, and $\overline{N}_{CB}$ is the number of DOFs in the reduced model of CB method.

Using the eigenvectors in Eq. (3.15), the global displacement vector $\mathbf{u}_g$ can be approximated by as

$$\mathbf{u}_g \approx \overline{\mathbf{u}}_{CB} = \overline{\boldsymbol{\Phi}}_{CB}\overline{\mathbf{q}}_{CB} \tag{3.16}$$

where $\overline{\boldsymbol{\Phi}}_{CB}$ and $\overline{\mathbf{q}}_{CB}$ are the reduced eigenvector matrix and its generalized coordinate vector, respectively.

3.3 Enhanced Craig-Bampton (ECB) method

From Eq. (3.12), the global displacement $\mathbf{u}_g$ can be exactly represented as

$$\mathbf{u}_g = \mathbf{T}_{CB}\mathbf{u}_{CB}, \tag{3.17a}$$

$$\mathbf{T}_{CB} = \begin{bmatrix} \boldsymbol{\Phi}_d & \boldsymbol{\Phi}_r & \boldsymbol{\Psi}_c \\ \mathbf{0} & \mathbf{0} & \mathbf{I}_b \end{bmatrix}, \ \mathbf{u}_{CB} = \begin{Bmatrix} \mathbf{q}_d \\ \mathbf{q}_r \\ \mathbf{u}_b \end{Bmatrix}, \tag{3.17b}$$

where $\mathbf{T}_{CB}$ and $\mathbf{u}_{CB}$ are the global transformation matrix and its generalized coordinate vector.

Using $\mathbf{T}_{CB}$ in Eq. (3.17), we can obtain the equations of motion for global structure

$$\left[\frac{d^2}{dt^2}\mathbf{M}_{CB} + \mathbf{K}_{CB}\right]\mathbf{u}_{CB} = \mathbf{0}, \tag{3.18a}$$

$$\mathbf{M}_{CB} = \mathbf{T}_{CB}^T\mathbf{M}_g\mathbf{T}_{CB}, \ \mathbf{K}_{CB} = \mathbf{T}_{CB}^T\mathbf{K}_g\mathbf{T}_{CB}, \tag{3.18b}$$

where $\mathbf{M}_{CB}$ and $\mathbf{K}_{CB}$ are global component mass and stiffness matrices, and the components of Eq. (3.18b) and Eq. (3.18c) are defined by

For harmonic response ($d^2(\ \ )/dt^2 = -\lambda$), Eq. (3.18a) can be rewritten as

$$\begin{bmatrix} \boldsymbol{\Lambda}_d - \lambda\mathbf{I}_d & \mathbf{0} & -\lambda\boldsymbol{\Phi}_d^T\hat{\mathbf{M}}_c \\ \mathbf{0} & \boldsymbol{\Lambda}_r - \lambda\mathbf{I}_r & -\lambda\boldsymbol{\Phi}_r^T\hat{\mathbf{M}}_c \\ -\lambda\hat{\mathbf{M}}_c^T\boldsymbol{\Phi}_d & \lambda\hat{\mathbf{M}}_c^T\boldsymbol{\Phi}_r & \hat{\mathbf{K}}_b - \lambda\hat{\mathbf{M}}_b \end{bmatrix}\begin{Bmatrix} \mathbf{q}_d \\ \mathbf{q}_r \\ \mathbf{u}_b \end{Bmatrix} = \mathbf{0}, \tag{3.19}$$

where the components of Eq. (3.19) are defined by

$$\mathbf{I}_d = \boldsymbol{\Phi}_d^T\mathbf{M}_s\boldsymbol{\Phi}_d, \ \mathbf{I}_r = \boldsymbol{\Phi}_r^T\mathbf{M}_s\boldsymbol{\Phi}_r, \tag{3.20a}$$

$$\boldsymbol{\Lambda}_d = \boldsymbol{\Phi}_d^T\mathbf{K}_s\boldsymbol{\Phi}_d, \ \boldsymbol{\Lambda}_d = \boldsymbol{\Phi}_d^T\mathbf{K}_s\boldsymbol{\Phi}_d, \tag{3.20b}$$

$$\hat{\mathbf{M}}_c = [\mathbf{M}_c - \mathbf{M}_s\mathbf{K}_s^{-1}\mathbf{K}_c], \tag{3.20c}$$

$$\hat{\mathbf{M}}_b = \mathbf{M}_b + \boldsymbol{\Psi}_c^T\mathbf{M}_c + \mathbf{M}_c^T\boldsymbol{\Psi}_c + \boldsymbol{\Psi}_c^T\mathbf{M}_s\boldsymbol{\Psi}_c, \tag{3.20d}$$

$$\hat{\mathbf{K}}_b = \mathbf{K}_b - \mathbf{K}_c^T\mathbf{K}_s^{-1}\mathbf{K}_c. \tag{3.20e}$$

Note that Eq. (3.20a) and Eq. (3.20b) denote the mass-orthonormality and the stiffness-orthogonality of structural eigenvectors, respectively.

From the second row in Eq. (3.19), we can obtain following relation as

$$[\mathbf{\Lambda}_r - \lambda \mathbf{I}_r]\mathbf{q}_r - \lambda \mathbf{\Phi}_r^T \hat{\mathbf{M}}_c \mathbf{u}_b = \mathbf{0}, \tag{3.21a}$$

$$\mathbf{q}_r = \lambda [\mathbf{\Lambda}_r - \lambda \mathbf{I}_r]^{-1} \mathbf{\Phi}_r^T \hat{\mathbf{M}}_c \mathbf{u}_b . \tag{3.21b}$$

By substituting Eq. (3.21b) into Eq. (3.17a), $\mathbf{u}_s$ can be represented as

$$\mathbf{u}_s = \mathbf{\Phi}_d \mathbf{q}_d + \mathbf{\Psi}_c \mathbf{u}_b + \lambda \mathbf{\Phi}_r [\mathbf{\Lambda}_r - \lambda \mathbf{I}_r]^{-1} \mathbf{\Phi}_r^T \hat{\mathbf{M}}_c \mathbf{u}_b . \tag{3.22}$$

Note that it is difficult to solve Eq. (3.22) because of unknown eigenvalue λ.

Using Taylor's series, the inverse term of Eq. (3.22) can be expanded as

$$\mathbf{\Phi}_r [\mathbf{\Lambda}_r - \lambda \mathbf{I}_r]^{-1} \mathbf{\Phi}_r^T = \mathbf{\Phi}_r \mathbf{\Lambda}_r^{-1} \mathbf{\Phi}_r^T + \lambda \mathbf{\Phi}_r \mathbf{\Lambda}_r^{-2} \mathbf{\Phi}_r^T + \cdots , \tag{3.23}$$

and then, by substituting the first term of Eq. (3.23) into Eq. (3.22), $\mathbf{u}_s$ can be approximated by

$$\mathbf{u}_s \approx \mathbf{\Phi}_d \mathbf{q}_d + \mathbf{\Psi}_c \mathbf{u}_b + \lambda \mathbf{\Phi}_r \mathbf{\Lambda}_r^{-1} \mathbf{\Phi}_r^T \hat{\mathbf{M}}_c \mathbf{u}_b . \tag{3.24}$$

Note that the first and second terms of Eq. (3.24) is exactly same with those of Eq. (3.12) in CB method and the third term of Eq. (3.24) has unknown eigenvalue λ.

Kim and Lee [20] proposed that λ can be approximated by O'callahan's approach [3], which was used to improve Guyan reduction. From Eq. (3.14a), following relation can be obtained by

$$\lambda \mathbf{u}_b = \overline{\mathbf{M}}_{CB}^{-1} \overline{\mathbf{K}}_{CB} \mathbf{u}_b . \tag{3.25}$$

By substituting Eq. (3.25) into Eq. (3.24), $\mathbf{u}_g$ can be approximated by

$$\mathbf{u}_g \approx \overline{\mathbf{u}}_g = \overline{\mathbf{T}}_{ECB} \overline{\mathbf{u}}_{CB} , \tag{3.26a}$$

$$\overline{\mathbf{T}}_{ECB} = \overline{\mathbf{T}}_{CB} + \overline{\mathbf{T}}_r , \tag{3.26b}$$

$$\overline{\mathbf{T}}_r = \begin{bmatrix} \mathbf{0} & \mathbf{\Phi}_r \mathbf{\Lambda}_r^{-1} \mathbf{\Phi}_r^T [-\mathbf{M}_s \mathbf{K}_s^{-1} \mathbf{K}_c + \mathbf{M}_c] \\ \mathbf{0} & \mathbf{0} \end{bmatrix} \overline{\mathbf{M}}_{CB}^{-1} \overline{\mathbf{K}}_{CB} , \tag{3.26c}$$

where $\overline{\mathbf{T}}_{ECB}$ is the enhanced transformation matrix and $\overline{\mathbf{T}}_r$ is the residual transformation matrix which was proposed by Kim and Lee [20]. Note that the partitioned coordinate in ECB method is same with that of original CB method.

Using $\overline{\mathbf{T}}_{ECB}$ in Eq. (3.26c), we can obtain the reduced equations of motion for partitioned structure,

$$\overline{\mathbf{M}}_{ECB}\ddot{\overline{\mathbf{u}}}_{CB} + \overline{\mathbf{K}}_{ECB}\overline{\mathbf{u}}_{CB} = \mathbf{0}, \tag{3.27a}$$

$$\overline{\mathbf{M}}_{ECB} = \overline{\mathbf{T}}_{ECB}^{T}\mathbf{M}_g\overline{\mathbf{T}}_{ECB}, \ \overline{\mathbf{K}}_{ECB} = \overline{\mathbf{T}}_{ECB}^{T}\mathbf{K}_g\overline{\mathbf{T}}_{ECB}, \tag{3.27b}$$

where $\overline{\mathbf{M}}_{ECB}$ and $\overline{\mathbf{K}}_{ECB}$ are the reduced mass and stiffness matrices, respectively, and $\overline{\mathbf{u}}_{CB}$ is the reduced displacement vector.

Using $\overline{\mathbf{M}}_{ECB}$ and $\overline{\mathbf{K}}_{ECB}$ in Eq. (3.27b), the reduced eigenvalue problem can be represented as

$$[\overline{\mathbf{K}}_{ECB} - (\overline{\lambda}_{ECB})_j\overline{\mathbf{M}}_{ECB}]\{\overline{\boldsymbol{\varphi}}_{ECB}\}_j = \mathbf{0} \quad \text{for} \quad j = 1, 2, \cdots, \overline{N}_{ECB}, \tag{3.28}$$

where $(\overline{\lambda}_{ECB})_j$ and $\{\overline{\boldsymbol{\varphi}}_{ECB}\}_j$ is the j^{th} approximated eigenvalue and eigenvector, respectively, and $\overline{N}_{ECB}$ is the number of DOFs in the reduced model of ECB method.

Using the eigenvectors in Eq. (3.28), the global displacement vector $\mathbf{u}_g$ can be approximated by

$$\mathbf{u}_g \approx \overline{\mathbf{u}}_{ECB} = \overline{\boldsymbol{\Phi}}_{ECB}\overline{\mathbf{q}}_{ECB} \tag{3.29}$$

where $\overline{\boldsymbol{\Phi}}_{ECB}$ and $\overline{\mathbf{q}}_{ECB}$ are the reduced eigenvector matrix and its generalized coordinate vector, respectively.

Chapter 4. Higher-order Craig-Bampton method

4.1 Formulation

From the Eq. (3.17a) and Eq. (3.17b), the global displacement vector $\mathbf{u}_g$ can be rewritten as

$$\mathbf{u}_g = \mathbf{T}_0 \mathbf{u}_0 , \tag{4.1a}$$

$$\mathbf{u}_0 = \begin{Bmatrix} \mathbf{u}_s \\ \mathbf{u}_b \end{Bmatrix}, \quad \mathbf{T}_0 = \begin{bmatrix} \boldsymbol{\Phi}_d & \boldsymbol{\Phi}_r & \boldsymbol{\Psi}_c \\ \mathbf{0} & \mathbf{0} & \mathbf{I}_b \end{bmatrix}, \quad \mathbf{u}_0 = \begin{Bmatrix} \mathbf{q}_d \\ \mathbf{q}_r \\ \mathbf{u}_b \end{Bmatrix}, \tag{4.1b}$$

where $\mathbf{T}_0$ is the global transformation matrix, which structural eigenvector matrix can be decomposed into two parts, dominant and residual.

From the inverse term of Eq. (3.22), we can define the residual flexibility $\mathbf{F}$ as

$$\mathbf{F} = \boldsymbol{\Phi}_r \left[\boldsymbol{\Lambda}_r - \lambda \mathbf{I}_r \right]^{-1} \boldsymbol{\Phi}_r^{\mathrm{T}} = \mathbf{F}_1 + \lambda \mathbf{F}_2 + \cdots + \lambda^{n-1} \mathbf{F}_n \tag{4.2a}$$

$$\mathbf{F}_n = \boldsymbol{\Phi}_r \boldsymbol{\Lambda}_r^{-n} \boldsymbol{\Phi}_r^{\mathrm{T}} \tag{4.2b}$$

where Eq. (4.2a) is expanded by Taylor series and $\mathbf{F}_n$ is the n^{th} order residual flexibility.

By substituting Eq. (4.2a) into Eq. (3.22), $\mathbf{u}_s$ can be represented as

$$\mathbf{u}_s = \boldsymbol{\Phi}_d \mathbf{q}_d + \boldsymbol{\Psi}_c \mathbf{u}_b + \boldsymbol{\Theta}_1 \boldsymbol{\eta}_1 + \cdots + \boldsymbol{\Theta}_k \boldsymbol{\eta}_k \quad \text{for} \quad k = 1, 2, \cdots, \infty \tag{4.3a}$$

$$\boldsymbol{\Theta}_k = \mathbf{F}_k \hat{\mathbf{M}}_c , \quad \boldsymbol{\eta}_k = \lambda^k \mathbf{u}_b \tag{4.3b}$$

where $\boldsymbol{\Theta}_k$ and $\boldsymbol{\eta}_k$ are the k^{th} order residual mode matrix and its generalized coordinate vector, respectively. Note that $\boldsymbol{\eta}_k$ is an additional coordinate vector containing the unknown eigenvalue (λ).

As mentioned previously, $\boldsymbol{\Phi}_d$ has been normalized with respect to $\mathbf{M}_s$. On the other hands, $\boldsymbol{\Theta}_k$ has arbitrary amplitude without normalization. Thus, $\boldsymbol{\Theta}_k$ also need a normalization process, otherwise $\boldsymbol{\Theta}_k$ may cause the transformation matrix badly scaled ($\boldsymbol{\Phi}_d, \boldsymbol{\Psi}_c >> \boldsymbol{\Theta}_k$). It may be desirable to normalize each column using its 2-norm [24,25].

$$\hat{\boldsymbol{\Theta}}_k = \boldsymbol{\Theta}_k \mathbf{G}_k^{-1} \tag{4.4a}$$

$$\mathbf{G}_k = \begin{bmatrix} \left\| \{\boldsymbol{\theta}_k\}_1 \right\|_2 & & \mathbf{0} \\ & \left\| \{\boldsymbol{\theta}_k\}_2 \right\|_2 & \\ & & \ddots \\ \mathbf{0} & & \left\| \{\boldsymbol{\theta}_k\}_{N_b} \right\|_2 \end{bmatrix} \tag{4.4b}$$

where $\mathbf{G}_k$ is a weighting matrix for $\boldsymbol{\Theta}_k$ and $\{\boldsymbol{\theta}_k\}_j$ is the j^{th} column of $\boldsymbol{\Theta}_k$.

In Eq. (4.3a), considering to the n^{th} order residual flexibility matrix $\mathbf{F}_n$, substructural displacement vector $\mathbf{u}_s$ is approximated as

$$\overline{\mathbf{u}}_s \approx \boldsymbol{\Phi}_s \mathbf{q}_d + \boldsymbol{\Psi}_c \mathbf{u}_b + \hat{\boldsymbol{\Theta}}_1 \boldsymbol{\eta}_1 + \cdots + \hat{\boldsymbol{\Theta}}_n \boldsymbol{\eta}_n \tag{4.5}$$

where $\overline{\mathbf{u}}_s$ is approximated by the n^{th} order residual flexibility.

Using Eq. (4.5), reduced equations of motion with n^{th} order residual flexibility can be obtained by

$$\mathbf{u}_g \approx \overline{\mathbf{u}}_g = \overline{\mathbf{T}}_n \overline{\mathbf{u}}_n, \tag{4.6a}$$

$$\overline{\mathbf{T}}_n = \left[\begin{array}{cc:ccc} \boldsymbol{\Phi}_d & \boldsymbol{\Psi}_c & \hat{\boldsymbol{\Theta}}_1 & \cdots & \hat{\boldsymbol{\Theta}}_n \\ \mathbf{0} & \mathbf{I}_b & \mathbf{0} & \cdots & \mathbf{0} \end{array}\right], \quad \overline{\mathbf{u}}_n = \begin{Bmatrix} \mathbf{q}_d \\ \mathbf{u}_b \\ \boldsymbol{\eta}_1 \\ \vdots \\ \boldsymbol{\eta}_n \end{Bmatrix}, \tag{4.6b}$$

where $\overline{\mathbf{T}}_n$ and $\overline{\mathbf{u}}_n$ are the reduced transformation matrix with n^{th} order residual flexibility and its generalized coordinate, respectively. Here, subscript *n* denotes the n^{th} order. Note that Eq. (4.6b) without residual flexibility is exactly same with Eq. (3.13b). In other words, HCB method with 0^{th} order residual flexibility (HCB-0) denotes the original CB method.

Using $\overline{\mathbf{T}}_n$ in Eq. (21), we can obtain the reduced equation of motion as

$$\overline{\mathbf{M}}_n \ddot{\overline{\mathbf{u}}}_n + \overline{\mathbf{K}}_n \overline{\mathbf{u}}_n = \mathbf{0}, \tag{4.7a}$$

$$\overline{\mathbf{M}}_n = \overline{\mathbf{T}}_n^T \mathbf{M}_g \overline{\mathbf{T}}_n, \quad \overline{\mathbf{K}}_n = \overline{\mathbf{T}}_n^T \mathbf{K}_g \overline{\mathbf{T}}_n, \tag{4.7b}$$

where $\overline{\mathbf{M}}_n$ and $\overline{\mathbf{K}}_n$ are the reduced mass and stiffness matrices, respectively. Note that the reduced model has the additional generalized coordinates $\boldsymbol{\eta}_1, \cdots, \boldsymbol{\eta}_n$.

The additional coordinates can be eliminated by SEREP [4], which is a DOFs-based reduction method without accuracy loss. Using SEREP, the reduced system in Eq. (4.7) can be reduced again, of which size is same with that of reduced system in Eq. (3.14).

From Eq. (4.7b), the following eigenvalue problem is obtained by

$$\overline{\mathbf{K}}_n\{\overline{\boldsymbol{\varphi}}_n\}_j = (\overline{\lambda}_n)_j \overline{\mathbf{M}}_n\{\overline{\boldsymbol{\varphi}}_n\}_j \quad \text{for} \quad j = 1, 2, \cdots, \overline{N}_n . \tag{4.8}$$

Using the results in Eq. (4.8), eigenvector matrix is defined by

$$\boldsymbol{\Phi}_n = [\,\{\overline{\boldsymbol{\varphi}}_n\}_1 \quad \{\overline{\boldsymbol{\varphi}}_n\}_2 \quad \cdots \quad \{\overline{\boldsymbol{\varphi}}_n\}_{\overline{N}_0} \,\vdots\, \{\overline{\boldsymbol{\varphi}}_n\}_{\overline{N}_0+1} \quad \cdots \quad \{\overline{\boldsymbol{\varphi}}_n\}_{\overline{N}_n}\,], \tag{4.9}$$

where $(\overline{\lambda}_n)_j$ and $\{\boldsymbol{\varphi}_p\}_j$ are the eigenvalue and eigenvector, respectively.

Considering to the $\overline{N}_0^{\text{th}}$ modes in $\boldsymbol{\Phi}_n$, we can reduce the transformation matrix $\overline{\mathbf{T}}_n$ with same matrix size with $\overline{\mathbf{T}}_0$ ($N_g \times \overline{N}_0$ matrix) as follows:

$$\tilde{\overline{\mathbf{T}}}_n = \overline{\mathbf{T}}_n \boldsymbol{\Phi}_n , \tag{4.10}$$

where $\tilde{\overline{\mathbf{T}}}_n$ is the transformation matrix in the HCB method, and its matrix size is $N_g \times \overline{N}_0$.

Using $\tilde{\overline{\mathbf{T}}}_n$ in Eq. (4.10), the reduced matrices of the HCB method is obtained by

$$\tilde{\overline{\mathbf{M}}}_n = \tilde{\overline{\mathbf{T}}}_n^T \mathbf{M}_g \tilde{\overline{\mathbf{T}}}_n , \;\; \tilde{\overline{\mathbf{K}}}_n = \tilde{\overline{\mathbf{T}}}_n^T \mathbf{K}_g \tilde{\overline{\mathbf{T}}}_n , \tag{4.11}$$

in which $\tilde{\overline{\mathbf{M}}}_n$ and $\tilde{\overline{\mathbf{K}}}_n$ are $\overline{N}_0 \times \overline{N}_0$ matrices.

Finally, the reduced eigenvalue problem in HCB method is given by

$$\tilde{\overline{\mathbf{K}}}_n(\overline{\boldsymbol{\varphi}})_i = \overline{\lambda}_i \tilde{\overline{\mathbf{M}}}_n (\overline{\boldsymbol{\varphi}})_i \quad \text{for} \quad i = 1, 2, \cdots, \overline{N}_0 \tag{4.12}$$

where $\overline{\lambda}_i$ and $(\overline{\boldsymbol{\varphi}})_i$ are the approximated eigenvalue and eigenvectors, respectively.

A key idea of the present derivation is considering the residual flexibility to improve the accuracy, dealing with unknown eigenvalue to make the components of transformation matrix identified and eliminating additional coordinates to reduce the size of system. Finally, the reduced system is more accurate without increasing size.

If increasing the order of residual flexibility, the reduced system is more accurate. However, it may take more computational cost. In practical aspect, the first and second order of residual flexibility (HCB-1, HCB-2) are enough to get an improved system. Because HCB-1 and HCB-2 have better accuracy than CB and ECB without increasing computational cost. This issue will be discussed in next sections.

4.2 Numerical Examples

In this section, we compare the performance of present method (HCB-1, HCB-2) with conventional method (CB, ECB). Three structural problems are considered: rectangular plate, cylindrical solid, hyperboloid shell problems. Each problem is implemented by four methods using MATLAB. The frequency cut-off mode selection method is used to select the dominant eigenvectors, and the following relative eigenvalue error is used to measure the accuracy of four methods.

$$\xi_j = \frac{\left|\lambda_j - \overline{\lambda}_j\right|}{\lambda_j}, \tag{4.13}$$

where λ_j and $\overline{\lambda}_j$ the j^{th} exact eigenvalue calculated from global eigenvalue problem and approximated eigenvalue calculated from reduced eigenvalue problem, respectively, and ξ_j is the relative eigenvalue error calculated in Eq. (4.13).

4.2.1 Rectangular plate problem

We consider a rectangular plate with free boundary. Length L is 20.0 m, width B is 12.0 m, and thickness h is 0.08 m. Young's modulus E is 206 GPa, Poisson's ratio ν is 0.33, density ρ is 7850 kg/m^3. The N_g and N_d are listed in Table 4.1.

In this example, we additionally test the accuracy using the relative eigenvector errors to compare the relative eigenvalue and eigenvector errors.

$$\zeta_j = 1 - \frac{\left|\boldsymbol{\varphi}_j \cdot \overline{\boldsymbol{\varphi}}_j\right|}{\left\|\boldsymbol{\varphi}_j\right\|_2 \left\|\overline{\boldsymbol{\varphi}}_j\right\|_2}, \tag{4.14}$$

where ζ_j is the j^{th} relative eigenvector error.

Fig. 4.1 presents the rectangular plate problem 1 which is modeled by thin mesh pattern and partitioned into three substructures ($N_s = 3$). Fig. 4.2 presents the numerical results of rectangular plate problem 1: Fig. 4.2(a)

presents the relative eigenvalue errors and Fig. 4.2(b) presents the relative eigenvector errors. Table 4.1 presents the number of dominant modes of the rectangular plate problem 1. Table 4.2 and Table 4.3 show the detailed relative eigenvalue and eigenvector errors.

From Fig. 4.2, we can figure out that error tendencies are similar in relative eigenvalue and eigenvector errors, and it means that we have been obtained the reliable results. From Fig. 4.2, Table 4.2 and Table 4.3, we can figure out their accuracy such as follows: Firstly, ECB, HCB-1 and HCB-2 have definitely improved accuracy than CB. Secondly, ECB and HCB-1 converge into a similar accuracy, and HCB-1 has slightly better accuracy than ECB. Thirdly, HCB-2 has similar accuracy at lower mode numbers with ECB and HCB-1, and HCB-2 has significantly improved accuracy at higher mode number than ECB and HCB-1.

Table 4.1. The number of dominant modes for the rectangular plate problem 1.

	$N_d^{(1)}$	$N_d^{(2)}$	$N_d^{(3)}$	N_d	N_g
Case (a)	13	7	5	25	1,365
Case (b)	13	7	5	25	1,365

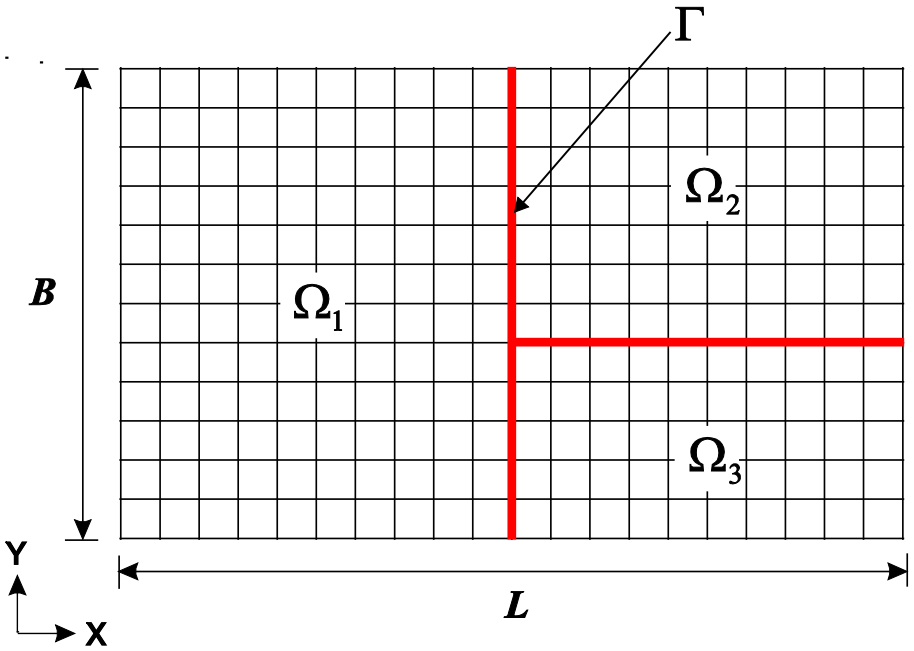

Fig. 4.1. Rectangular plate problem 1

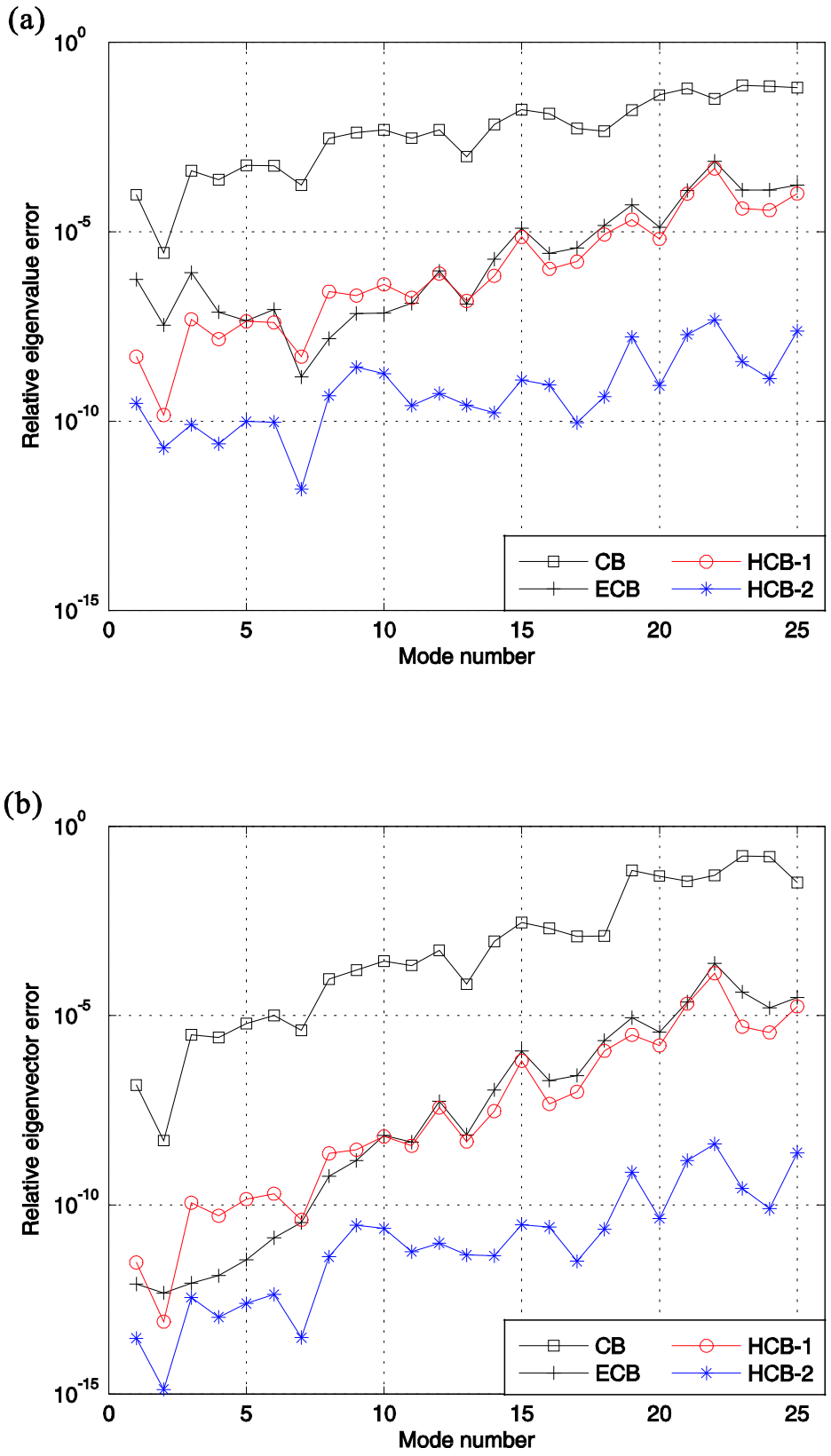

Fig. 4.2. Numerical results for the rectangular plate problem 1: (a) relative eigenvalue errors in $N_d = 25$ and (b) relative eigenvector errors in $N_d = 25$.

Table 4.2. The relative eigenvalue errors for the rectangular plate problem 1.

Mode number	CB	ECB	Present	
			HCB-1	HCB-2
1	9.415E-05	5.002E-07	5.005E-09	2.959E-10
2	2.728E-06	8.761E-09	1.427E-10	1.950E-11
3	4.116E-04	2.025E-07	4.866E-08	8.009E-11
4	2.340E-04	2.197E-08	1.457E-08	2.506E-11
5	5.675E-04	4.546E-08	4.259E-08	9.764E-11
6	5.586E-04	1.249E-08	4.047E-08	9.358E-11
7	1.717E-04	2.960E-09	5.021E-09	1.588E-12
8	2.912E-03	1.219E-08	2.600E-07	4.676E-10
9	4.129E-03	6.508E-08	2.054E-07	2.649E-09
10	4.914E-03	1.323E-07	4.067E-07	1.798E-09
11	2.972E-03	1.375E-07	1.792E-07	2.574E-10
12	4.866E-03	9.119E-07	7.829E-07	5.316E-10
13	9.609E-04	1.271E-07	1.477E-07	2.608E-10
14	6.775E-03	1.882E-06	6.818E-07	1.666E-10
15	1.662E-02	1.236E-05	7.281E-06	1.207E-09
16	1.306E-02	2.638E-06	1.051E-06	8.905E-10
17	5.277E-03	3.759E-06	1.610E-06	9.068E-11
18	4.522E-03	1.441E-05	8.445E-06	4.373E-10
19	1.627E-02	5.038E-05	2.083E-05	1.653E-08
20	4.090E-02	1.305E-05	6.466E-06	8.669E-10
21	6.032E-02	1.227E-04	1.002E-04	1.923E-08
22	3.275E-02	7.298E-04	4.724E-04	4.747E-08
23	7.284E-02	1.260E-04	4.135E-05	3.747E-09
24	7.013E-02	1.250E-04	3.734E-05	1.310E-09
25	6.422E-02	1.694E-04	1.021E-04	2.382E-08

Table 4.3. The relative eigenvector errors for the rectangular plate problem 1.

Mode number	CB	ECB	Present	
			HCB-1	HCB-2
1	1.429E-07	7.997E-13	3.008E-12	3.009E-14
2	4.973E-09	4.745E-13	8.260E-14	1.332E-15
3	3.101E-06	8.525E-13	1.142E-10	3.552E-13
4	2.618E-06	1.336E-12	5.134E-11	1.079E-13
5	6.055E-06	3.559E-12	1.433E-10	2.471E-13
6	9.902E-06	1.332E-11	1.975E-10	4.349E-13
7	4.110E-06	3.384E-11	4.039E-11	3.109E-14
8	9.132E-05	5.692E-10	2.261E-09	4.186E-12
9	1.583E-04	1.463E-09	2.852E-09	2.894E-11
10	2.764E-04	6.757E-09	6.373E-09	2.366E-11
11	2.088E-04	4.480E-09	3.594E-09	5.769E-12
12	5.263E-04	5.381E-08	3.666E-08	9.788E-12
13	6.677E-05	7.018E-09	4.683E-09	4.722E-12
14	9.024E-04	1.080E-07	3.000E-08	4.493E-12
15	2.870E-03	1.152E-06	6.370E-07	3.000E-11
16	2.002E-03	1.928E-07	4.611E-08	2.592E-11
17	1.221E-03	2.601E-07	9.560E-08	3.215E-12
18	1.257E-03	2.198E-06	1.173E-06	2.265E-11
19	6.781E-02	8.807E-06	3.063E-06	7.315E-10
20	4.820E-02	3.663E-06	1.618E-06	4.363E-11
21	3.495E-02	2.291E-05	2.057E-05	1.476E-09
22	5.056E-02	2.379E-04	1.297E-04	4.059E-09
23	1.611E-01	4.190E-05	5.092E-06	2.720E-10
24	1.560E-01	1.580E-05	3.584E-06	7.889E-11
25	3.241E-02	2.952E-05	1.753E-05	2.383E-09

4.2.2 Cylindrical solid problem

We consider a cylindrical solid with free boundary. Lengths L_1 and L_2 are 0.16 m and 0.24 m, respectively, and the radii R_1, R_2 and R_3 are 0.08 m, 0.12 and 0.16 m, respectively. Young's modulus E is 76 GPa, Poisson's ratio ν is 0.33 and density ρ is 2,796 kg/m^3. The cylindrical solid problem is modeled using 8-node brick elements and partitioned into four substructures ($N_s = 4$). N_g and N_d are listed in Table 4.4. Fig. 4.3 presents the cylindrical problem and Fig. 4.4 presents its relative eigenvalue errors in two different cases.

Table 4.4 The number of dominant modes for the cylindrical solid problem.

	$N_d^{(1)}$	$N_d^{(2)}$	$N_d^{(3)}$	$N_d^{(4)}$	N_d	N_g
Case (a)	3	3	3	3	12	1,740
Case (b)	5	5	5	5	20	1,740

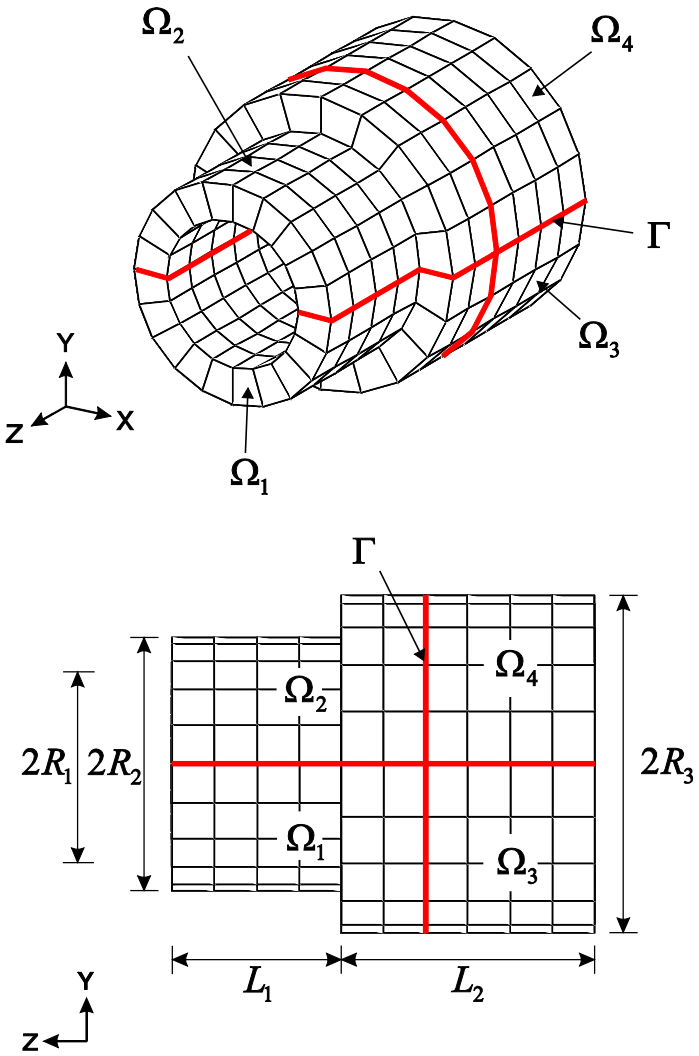

Fig. 4.3. Cylindrical solid problem

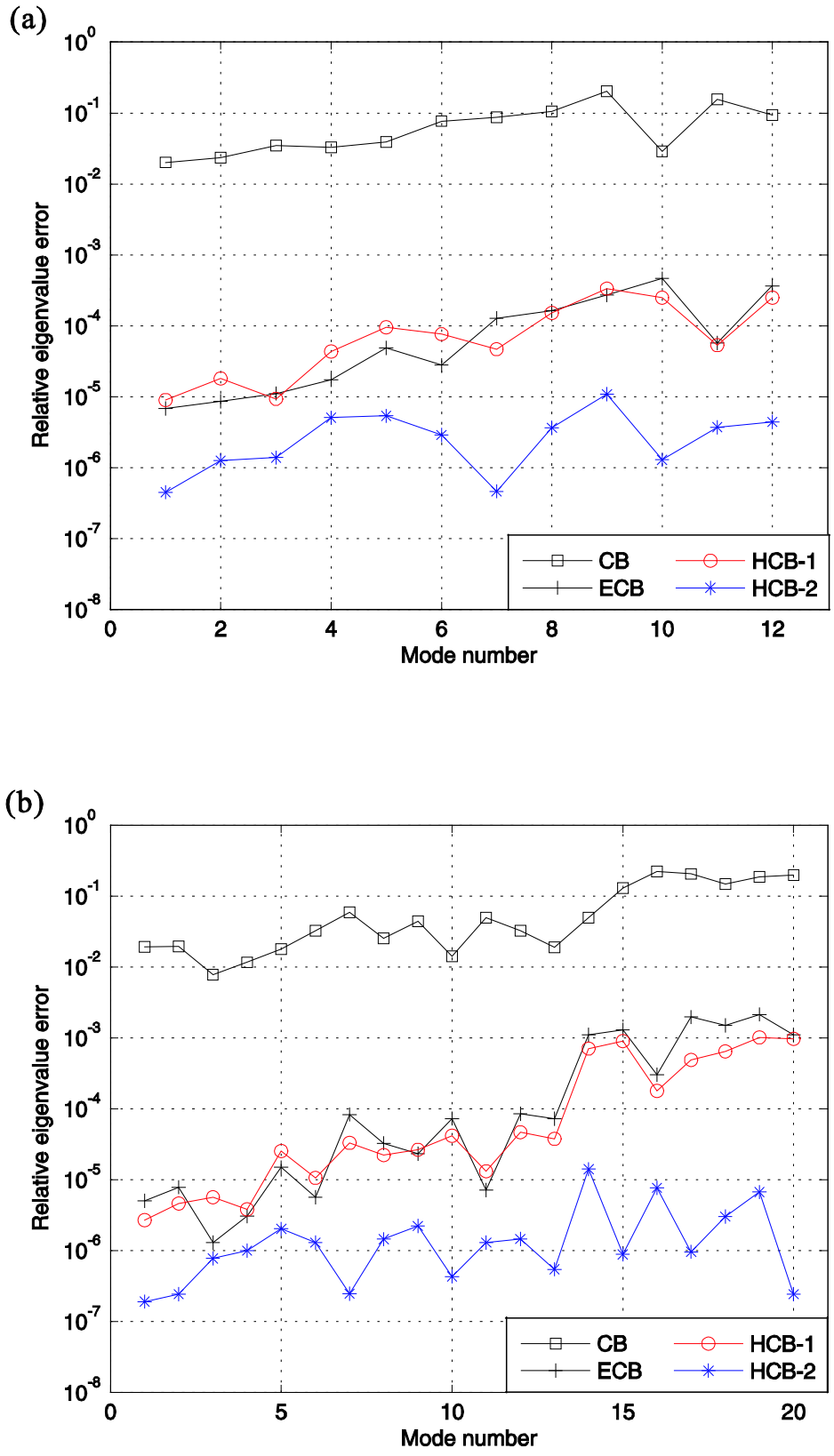

Fig. 4.4. Numerical results for the cylindrical solid problem: (a) relative eigenvalue errors in $N_d = 12$ (b) relative eigenvalue errors in $N_d = 20$.

4.2.3 Cylindrical panel problem

We consider a cylindrical panel with free boundary. Length L is 0.8 m, radius R is 0.5 m, and thickness h is 0.005 m. Young's modulus E is 69 GPa, Poisson's ratio ν is 0.35, and density ρ is 2,700 kg/m^3. Each edge is discretized in the following ratio:

$$L_1 : L_2 : L_3 : \cdots : L_{16} = 16 : 15 : 15 : \cdots : 1, \tag{4.15}$$

The cylindrical panel is modeled by a 16×16 distorted mesh of finite shell elements and partitioned into four substructures($N_s = 7$). N_g and N_d are listed in Table 4.5. Fig. 4.5 presents the cylindrical panel problem and Fig. 4.6 presents its the relative eigenvalue errors in two different cases.

Table 4.5. The number of dominant modes for the cylindrical panel problem.

	$N_d^{(1)}$	$N_d^{(2)}$	$N_d^{(3)}$	$N_d^{(4)}$	$N_d^{(5)}$	$N_d^{(6)}$	$N_d^{(7)}$	N_d	N_g
Case (a)	2	2	2	2	4	4	4	20	1,445
Case (b)	4	4	4	4	8	8	8	40	1,445

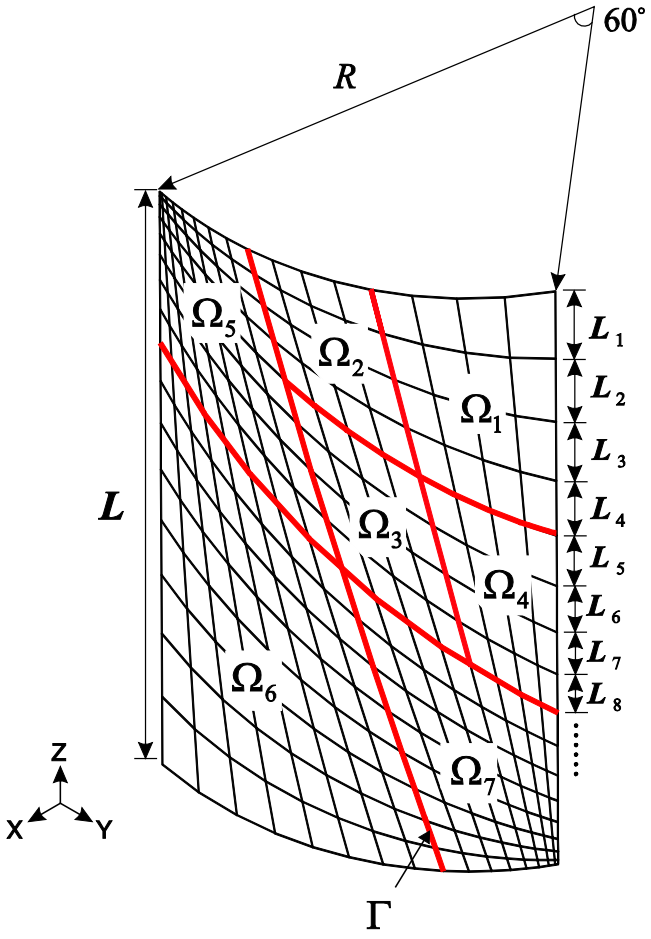

Fig. 4.5. Cylindrical panel problem with a distorted mesh

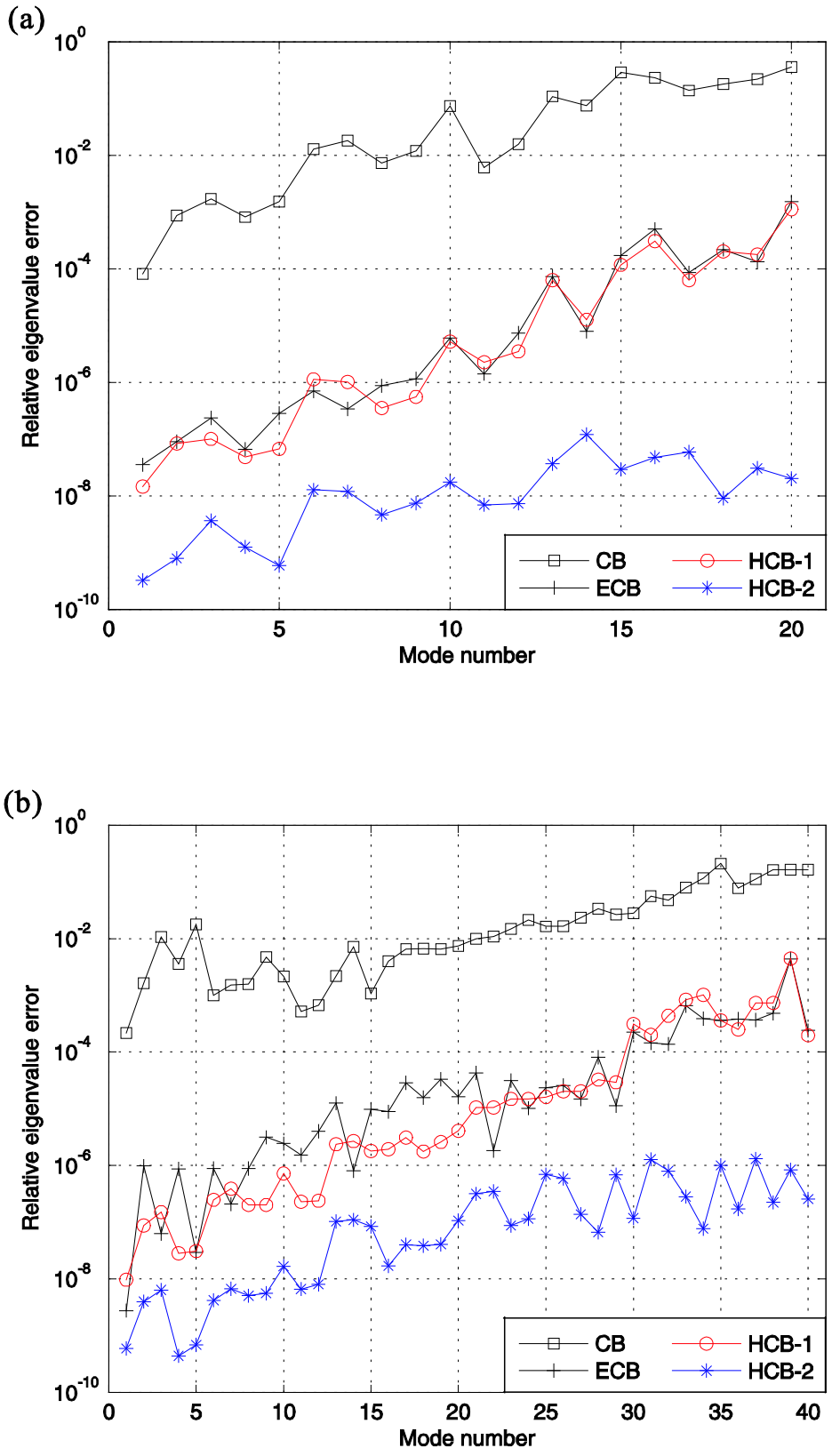

Fig. 4.6. Numerical results for the cylindrical panel problem: (a) relative eigenvalue errors in $N_d = 20$ (b) relative eigenvalue errors in $N_d = 40$.

4.2.4 Hyperboloid shell problem

We consider a hyperboloid shell with free boundary. Height H is 4.0 m and thickness h is 0.05 m. Young's modulus E is 69 GPa, Poisson's ratio ν is 0.35, and density ρ is 2,700 kg/m^3. The mid-surface of this shell structure is described by

$$x^2 + y^2 = 2 + z^2; \quad z \in [-2,2], \tag{4.16}$$

The hyperboloid shell problem is modeled using 4-node MITC shell elements and partitioned into four sub-structures ($N_s = 8$). N_g and N_d are listed in Table 4.6. Fig. 4.7 presents the cylindrical problem and Fig. 4.8 presents its relative eigenvalue errors in two different cases.

Table 4.6. The number of dominant modes for the hyperboloid shell problem.

	$N_d^{(1)}$	$N_d^{(2)}$	$N_d^{(3)}$	$N_d^{(4)}$	$N_d^{(5)}$	$N_d^{(6)}$	$N_d^{(7)}$	$N_d^{(8)}$	N_d	N_g
Case (a)	3	3	3	3	3	3	3	3	24	4,200
Case (b)	4	4	4	4	4	4	4	4	32	4,200

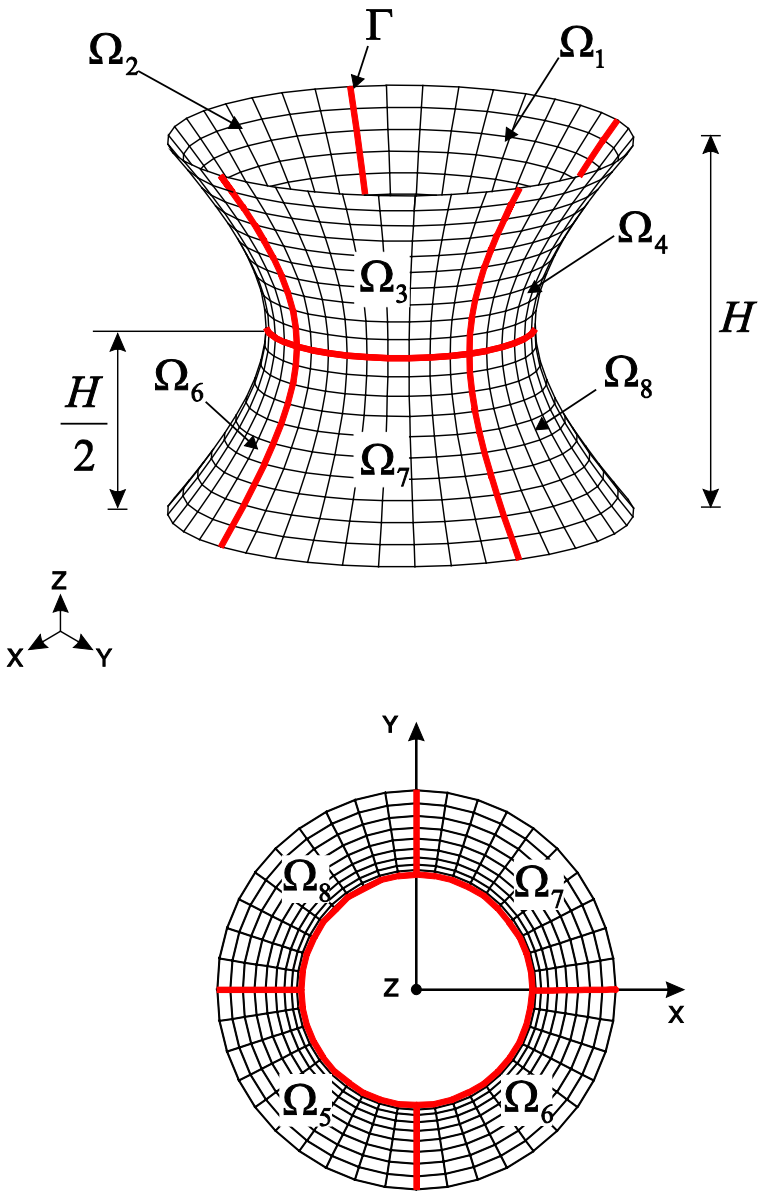

Fig. 4.7. Hyperboloid shell problem

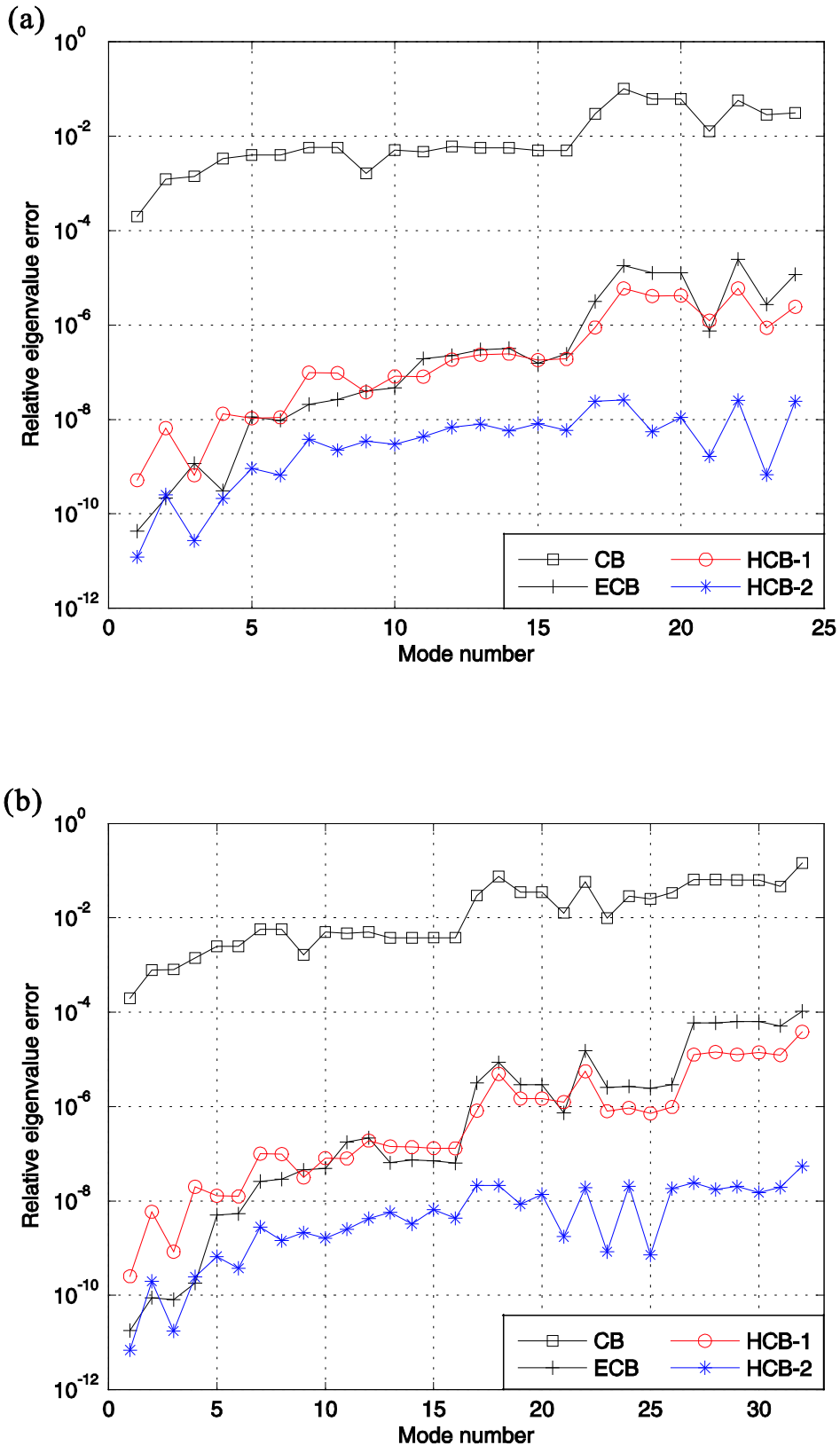

Fig. 9. Numerical results for the hyperboloid shell problems: (a) relative eigenvalue errors in $N_d = 24$ (b) relative eigenvalue errors in $N_d = 32$.

5. Computational cost

In this section, we test the computational cost of present methods (HCB-1, HCB-2) with conventional methods (CB, ECB). Here, the rectangular plate problem 2 is considered, which has the same material properties with rectangular plate problem 1. Fig. 5.1 presents the rectangular plate problem 2 which is modeled by dense mesh pattern and partitioned into four substructures ($N_s = 4$). N_g and N_d are listed in Table 5.1. Fig. 5.2 presents the relative errors of rectangular plate problem 2.

To test the computational cost, we established a criterion that the relative eigenvalue errors in lower than mode number 200 have less than 10^{-3}. Fig 5.2 shows that all methods satisfy the criterion. Note that present methods have better accuracy in lower modes and it means that the test has been performed conservatively.

All the code implementations are done using MATLAB in a personal computer (Inter core (TM) i7-3770, 3.40 GHz CPU, 32 GB RAM). Table 5.2 present the detailed computational times and their ratio. Even though an unfavorable condition, the present methods have a better accuracy and take a less computational time.

Table 5.1. The number of dominant modes for the rectangular plate problem 2.

	$N_d^{(1)}$	$N_d^{(2)}$	$N_d^{(3)}$	$N_d^{(4)}$	N_d	N_g
CB	400	400	400	400	1,200	11,285
ECB	75	75	75	75	300	11,285
HCB-1	75	75	75	75	300	11,285
HCB-2	50	50	50	50	200	11,285

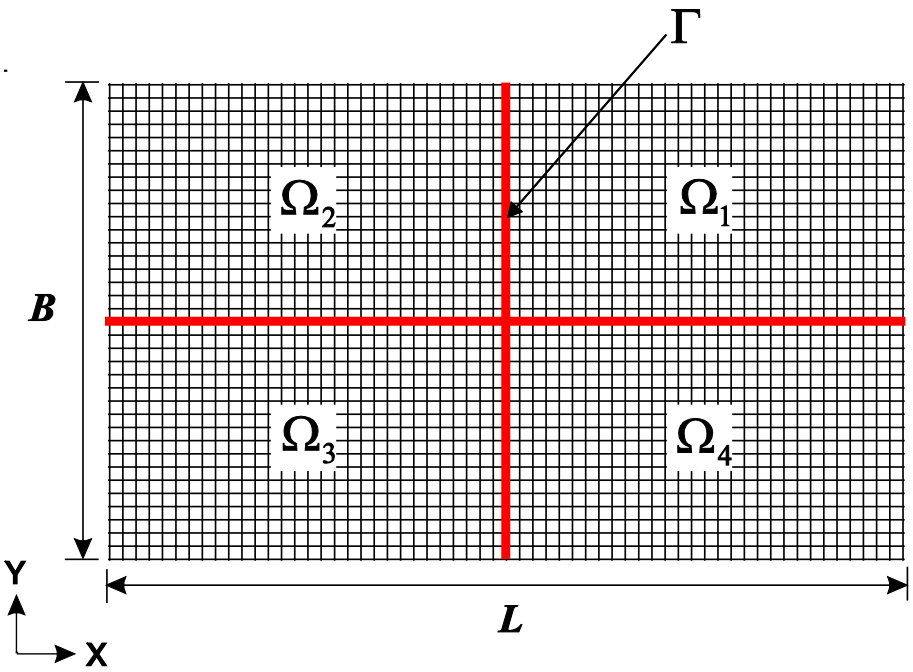

Fig. 5.1. Rectangular plate problem 2

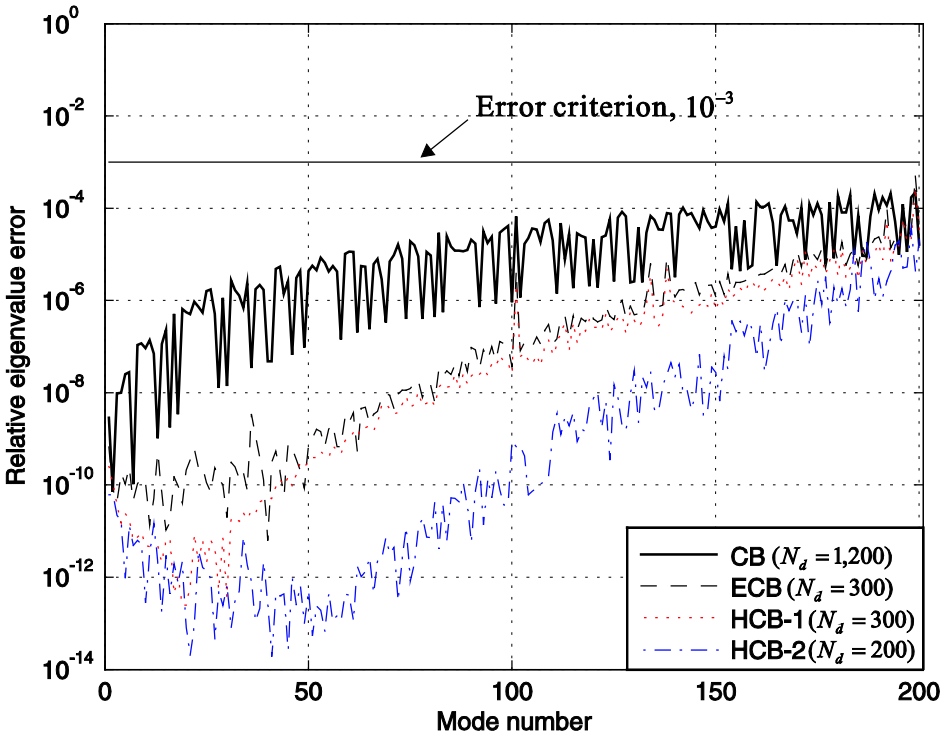

Fig. 5.2. Relative eigenvalue errors for the rectangular plate problem 2.

Table 5.2. Computation cost for the rectangular plate problem 2.

	Computation times	
	CPU time [sec]	Ratio [%]
CB	242.95	100
ECB	65.06	26.77
HCB-1	78.38	32.26
HCB-2	113.92	46.89

6. Conclusion

In this study, we developed a new component mode synthesis method by improving CB method. In HCB method, the unknown coefficients of residual flexibility were considered in generalized coordinates to make the components of transformation matrix known. And then, undesirable coordinates which has unknown variables were eliminated by additional transformation matrix. As a result, we obtained the new component matrices of which accuracy is significantly improved.

If we consider the more orders of residual flexibility, then we would obtain the reduced model more precisely. However, in practical aspects, we considered the first- and second-order residual flexibility. The improved performance of HCB-1 and HCB-2 was verified through various numerical examples.

Using HCB method, global (original) structural models can be more precisely reduced, and the accuracy of reduced models is significantly improved. The accuracy improvement of HCB method was demonstrated through numerical examples, and its computational cost was also investigated.

References

[1] Craig RR, Kurdila AJ. Fundamentals of structural dynamics. John Wiley & Sons, 2006.

[2] Bathe KJ. Finite element procedure, 2006

[2] Hurty, W. C. Dynamic analysis of structural systems using component modes. AIAA J 1965;3(4):678-685.

[3] Craig RR, Bampton MCC. Coupling of substructures for dynamic analysis. AIAA J 1968;6(7):1313-9.

[4] Benfield WA, Hruda RF. Vibration analysis of structures by component mode substitution. AIAA J 1971;9:1255-61.

[5] Rubin S. Improved component-mode representation for structural dynamic analysis. AIAA J 1975;13(8):995-1006.

[6] Hintz RM. Analytical Methods in Component Modal Synthesis, AIAA J 1975;13(8):1007-1016.

[7] Craig RR, Hale AL. Block-Krylov component mode synthesis method for structural model reduction. AIAA J 1988;11(6):562-70

[8] Craig RR, Substructure method in vibration. J Vib Acoust 1995;117(B):207-13.

[9] MacNeal RH, Hybrid method of component mode synthesis. Comput Struct 1971;1(4):581-601

[10] Bourquin F. Component mode synthesis and eigenvalues of second order operators: discretization and algorithm. Math Model Numer Anal 1992;26(3):385-423

[11] Rixen DJ. Adual Craig-Bampton method for dynamic substructuring. J Comput Appl Math 2004;168(1-2):383-91.

[12] Bennighof JK. Lehoucq RB. An automated multi-level substructuring method for eigenspace computation in linear elastodynamics. SIAM J Sci Comput 2004;25(6):2084-106.

[13] Park KC, Park YH. Partitioned component mode synthesis via a flexibility approach. AIAA J 2004;42(6):1236-45.

[14] Kim JG, Lee PS. An enhanced Craig-Bampton method. Intl J Numer Methods Eng 2015; 103:79-93.

[15] Kim JG, Boo SH, Lee PS. An enhance AMLS method and its performance. Comput Methods Appl Mech Eng 2015;287:90-111.

[16] Baek SM. Study on the multi-level substructuring scheme and system condensation for the large-scaled

structural dynamic analysis [Ph.D. thesis]. Department of Mechanical and Aerospace Engineering, Seoul National University, 2012.

[17] Boo SH, Kim JG, Lee PS. A simplified error estimator for the CB method and its application to error control. Compt Struct 2016;164:53-62

[18] Lee PS, Bathe KJ. Development of MITC isotropic triangular shell finite elements. Comput Struct 2004;82(11-12):945-62.

[19] Lee PS, Bathe KJ. Development of MITC isotropic triangular shell finite elements. Comput Struct 2004;82(11-12):945-62.

[20] O'Callahan J. A procedure for an improved reduced system (IRS) model. Proceedings of the 7th International Modal Analysis Conference, Las Vegas, 1989:17-21.

[21] O'Callahan J, Avitabile P, Riemer R. System equivalent reduction expansion process (SEREP). Proceedings of the 7th International Modal Analysis Conference, Las Vegas, 1989:29-37.

요 약 문

고차 잔류 유연도를 활용한 부분 구조 합성법 개발

최근 컴퓨터의 기능이 비약적으로 발달함에 따라 구조동역학적 해석이 필요한 유한요소 모델이 점차 복잡해지고 대형화되고 있다. 이러한 이유로 해석에 필요한 전산 소요 비용(computational cost)이 급증하고 있다. 이러한 공학적 문제를 효율적으로 해결하기 위하여, 부분 구조 합성법이 주목받고 있다. 부분 구조 합성법은 원래의 유한요소 모델을 다루기 쉬운 여러 부분 구조로 분할한 뒤, 각 부분 구조의 자유도(DOFs)를 축소하여, 다시 합성함으로써 축소된 모델을 얻는 과정을 지칭한다. 이때 모델 축소법(Model reduction)에 사용되는 원리에 따라, 자유도 기반의 축소법(DOFs based)과 모드 기반의 축소법(Mode based)으로 구분된다.

자유도 기반의 축소법은 우선 전체 자유도 중에서 활성 자유도(Actived DOFs)와 삭제 자유도(Deleted DOFs)로 구분한다. 이후 삭제 자유도를 응축(Condensation)하여, 활성 자유도가 전체 구조물의 거동을 효율적으로 근사할 수 있도록 한다. 1965 년에 Guyan 이 정적 응축법(Static condensation)을 제안한 이후로 지속적인 관심을 받아 왔으며, 다양한 연구분야에서 적용되었다. 이후 1989 년에는 O'callahan 이 동적 응축법(Dynamic condensation)을 제안하여 더 정확한 축소법이 개발되었다. 1995 년 Friswell 이 반복적 축소법을 제안하였고, 최근에는 이에 기반한 연구가 활발하게 진행되고 있다. 이처럼 모델 축소법에 관한 연구는 더 정확한 축소모델을 개발하는 데에 초점이 맞춰져 있다.

모드 기반 축소법은 우선 고유치해석(eigenvalue analysis)을 실시하여 구조물의 모드를 분석한다. 이때 저차모드가 주요하다는 사실에 기인하여, 고차모드를 응축함으로써 저차모드가 전체 구조물의 거동을 효율적으로 근사할 수 있도록 한다. 모드 기반 축소법은 부구조법(Substructuring)의 적용으로 자유도 기반 축소법에 비해 향상된 성능을 보여주었다.

부구조법이 적용된 모드 기반 축소법을 부분 구조 합성법(Component mode synthesis, CMS)라 한다. 부분 구조 합성법의 개념은 1965 년 Hurty 에 의해 제시되었으며, 1968 년 Craig 와 Bampton 에 의해 최초의 부분 구조 합성 기법이 개발되었다. 이후 50 년간, 더 정확한 축소 모델을 개발하기 위해 다양한 형태의 부분 구조 합성법에 대한 연구가 진행되었으며, 본 연구도 동일한 연구 목적을 갖고 있다.

본 연구에서는 기존의 부분구조합성법에서 고려하지 않았던, 잔류 유연도(Residual flexibility)를 효율적으로 고려하는 방법을 제시하였다. 즉, 잔류 유연도를 적적하게 고려함으로써, 기존의 부분구조합성법의 정확성을 향상시킨 것이다. 또한, 본 연구에서는 잔류 유연도를 n 차의 항(n-th order)으로 구성하였으며, 고차 항(higher-order)을 고려할수록 정확도가 개선되는 것을 확인하였다. 또한, 본 연구에서 제안한 방법은 기존의 부분구조합성법과 동일한 크기로 모델을 축소시킨다. 즉, 축소 모델의 크기는 동일하면서 동시에 정확도를 대폭 개선한 것이다. 이러한 내용은 최종적으로 다양한 수치해석 예제를 통해 검증되었다.